UNCLASSIFIED

AD NUMBER
AD348405
CLASSIFICATION CHANGES
TO: **UNCLASSIFIED**
FROM: **CONFIDENTIAL**
LIMITATION CHANGES
TO: **Approved for public release; distribution is unlimited.**
FROM: **Controlling DoD Organization: Commanding Officer, U.S. Army Biological Laboratories, Fort Detrick, MD.**
AUTHORITY
OSD/WHS ltr dtd 1 Aug 2013; OSD/WHS ltr dtd 1 Aug 2013

THIS PAGE IS UNCLASSIFIED

#1

DECLASSIFIED IN FULL
Authority: EO 13526
Chief, Records & Declass Div, WHS
Date: JUL 19 2013

~~CONFIDENTIAL~~

AD 348405

DEFENSE DOCUMENTATION CENTER
FOR
SCIENTIFIC AND TECHNICAL INFORMATION
CAMERON STATION, ALEXANDRIA, VIRGINIA

Office of the Secretary of Defense 5USC. §552
Chief, RDD, ESD, WHS
Date: 19JUL2013 Authority: EO 13526
Declassify: X Deny in Full: ______
Declassify in Part: ______
Reason: ______
MDR: 12 -M- 3144

~~CONFIDENTIAL~~

12-M-3144

R-1

NOTICE: When government or other drawings, specifications or other data are used for any purpose other than in connection with a definitely related government procurement operation, the U. S. Government thereby incurs no responsibility, nor any obligation whatsoever; and the fact that the Government may have formulated, furnished, or in any way supplied the said drawings, specifications, or other data is not to be regarded by implication or otherwise as in any manner licensing the holder or any other person or corporation, or conveying any rights or permission to manufacture, use or sell any patented invention that may in any way be related thereto.

NOTICE:

[redacted]

348405

DECLASSIFIED IN FULL
Authority: EO 13526
Chief, Records & Declass Div, WHS
Date: JUL 19 2013

General Mills

THE GENERAL MILLS ELECTRONICS GROUP

CONFIDENTIAL

DECLASSIFIED IN FULL
Authority: EO 13526
Chief, Records & Declass Div, WHS
Date: JUL 19 2013

General Mills

~~CONFIDENTIAL~~

This document consists of 13 CONF. pages, and is number 27 of 49 copies, series A and the following ---- attachments.

FOURTEENTH QUARTERLY PROGRESS REPORT ON DISSEMINATION OF SOLID AND LIQUID BW AGENTS

(Unclassified Title)

For Period 4 September - 4 December 1963
Contract No. DA-18-064-CML-2745

Prepared for:

U. S Army Biological Laboratories
Fort Detrick, Maryland

MAR [illegible] 1964

Submitted by: G R Whitnah
G. R. Whitnah
Project Manager

Report No: 2512
Project No: 82408
Date: 3 February 1964

Approved by:
S. P. Jones, Director
Aerospace Research

AEROSPACE RESEARCH
2295 Walnut Street
St. Paul 13, Minnesota

[redacted]

[redacted]

~~CONFIDENTIAL~~

FOREWORD

Staff members of the Aerospace Research Department and Engineering Department who have participated in directing or performing the work reported herein include Messrs. S. P. Jones, Jr., G. Whitnah, M. Sandgren, A. Anderson, D. Stender, R. Lindquist, J. McGillicuddy, J. Upton, W. L. Torgeson, P. Stroom, G. Morfitt, A. T. Bauman, D. Harrington, R. Ackroyd, D. Kedl, B. Schmidt, G. Lunde, R. Dahlberg, E. Knutson, J. Ungs, J. Pilney, A. Johnson, G. Leiter, C. A. Morris, K. Pontinen, and G. Voll.

DDC AVAILABILITY NOTICE

[redacted]

[redacted]

[redacted]

ABSTRACT

This Fourteenth Quarterly Progress Report presents the results of work conducted at General Mills, Inc., under Contract No. DA-18-064-CML-2745, "Dissemination of Solid and Liquid BW Agents" during the period 4 September to 4 December 1963.

Current theoretical investigations relating the interparticle contact energies to mechanical properties of compacted powders are described. Although an idealized system was used, the trends predicted are in accord with experimental data.

Bg (lot SCH-63-109) to be used in forthcoming flight tests was found to be more difficult to compact than Bg (lot 17) used previously. A new approach to obtain the energy of compaction from Instron data is presented.

Agent LX like other highly elastic materials was found to be difficult to compact, has a comparatively high compaction shear strength, and a tensile strength too low to measure.

An evaluation was made of the buoyant force corrections for the BET adsorption method to measure total surface area. Total surface area and rugosity measurements were made for spray-dried saccharin, agent LX, and egg embryo.

Our methods for preparing shadow-cast samples for the electron microscope have resulted in obtaining micrographs showing greater detail in particle shapes.

A study of the effects of humidity (from 0 to 100 percent R. H.) upon the formation and decay of a ground powdered sugar aerosol is reported.

Storage tests on samples of compacted Sm indicate little change in deagglomeration efficiencies and viability after 6 months at temperatures of -2 and -23°C.

An experiment conducted using Mistron Vapor talc compacted in a 6-inch diameter tube wiped with graphite and lined with polyethylene film plastic indicated that side-wall friction can be materially reduced if suitable methods can be found for preventing intimate contact of the powder particles with the wall surface.

In preparation for the low-speed flight trials of the E-41 spray tank on the Mohawk OV-1C airplane, an E-41 was filled with compacted talc and shipped to Grumman Aircraft Engineering Corporation, Bethpage, Long Island, New York. A manual loading technique using partial charges was developed in anticipation of having to load the E-41 with Bg in the field during the flight trials.

TABLE OF CONTENTS

Page determined to be Unclassified
Reviewed Chief, RDD, WHS
IAW EO 13526, Section 3.5
Date: JUL 19 2013

TABLE OF CONTENTS (continued)

LIST OF ILLUSTRATIONS

LIST OF ILLUSTRATIONS (continued)

Page determined to be Unclassified
Reviewed Chief, RDD, WHS
IAW EO 13526, Section 3.5
Date: JUL 19 2013

LIST OF ILLUSTRATIONS (continued)

FOURTEENTH QUARTERLY PROGRESS REPORT
ON
DISSEMINATION OF SOLID AND LIQUID BW AGENTS

1. INTRODUCTION

The work reported herein is being conducted for the U. S. Army Biological Laboratories under Contract DA-18-064-CML-2745. The program consists of experimental and theoretical studies related to the line source dissemination of solid and liquid BW agents. For several months the emphasis has been placed on the dry agents; much effort is being devoted to the study of the processes and phenomena involved when dry agents are disseminated from a compacted state, in order to obtain a more favorable filling density in munitions. Processes involved in compacting agents to obtain the required densities are being included in the studies.

Work on the fundamental properties of dry finely-divided solid materials is being conducted in the laboratories. Special instrumentation required for these studies is designed and fabricated when necessary. Two full-scale E-41 spray tanks were fabricated and are being used in field tests to study the dissemination and dispersion of compacted dry agents under natural conditions. Flight tests at high subsonic speeds have been conducted successfully and preparations for low-speed tests are currently in process.

Progress in several areas of the program during the period 4 September through 4 December 1963 is presented in this report.

Page determined to be Unclassified
Reviewed Chief, RDD, WHS
IAW EO 13526, Section 3.5
Date: JUL 19 2013

2. STUDIES OF THE FUNDAMENTAL BEHAVIOR OF DRY POWDERS

During the course of this project we have been studying the bulk properties such as energy of compaction, shear strength, and tensile strength which are manifestations of interparticle contact energies. In addition, we have studied particle characteristics--such as size and shape--that affect the number and nature of the interparticle contacts.

The following sections describe the results of current theoretical investigations relating the interparticle contact energies to the mechanical properties of compacted powders. A theoretical model composed of spherical particles of diameter d_p with an average energy E per single contact is employed to determine the energy required to produce a given change in average powder density. This treatment should be of considerable value in adding to our depth of understanding of the behavior of powders. Although we are using an idealized system, the trends predicted are substantially in agreement with experimental results. In addition to the results of theoretical studies, our current work using Bg and other simulants is reported.

2.1. Behavior of Powders in the Compacted State

2.1.1. Theoretical Investigations of the Mechanics of Compacted Powders

Granular materials can be divided broadly into two main classes: dilatant media and compactable media. Dilatant materials are so named because they dilate or expand when sheared. Compactable materials, on the other hand, are found to contract when sheared. This distinction leads to fundamental differences in the behavior of dilatant and compactable materials. For example, a dilatant powder is capable of sustaining very large shear stresses if the powder is not permitted to expand. This phenomenon was demonstrated in an experiment reported by Jenkin[1] which showed that a cylinder imbedded in sand in a confined space could not be rotated in its plane. Similar behavior has been reported by Zenz and Othmer (See pp. 77, Reference 2). This type of behavior is not observed with compactable powders[*].

For the most part, dry dilatant powders flow freely and are not ordinarily subject to handling difficulties. By contrast, compactable powders do not flow readily and may present serious handling difficulties in certain circumstances.

We may ask: What factors determine whether a given powder will be dilatant or compactable? There is good reason to believe that the answer to this question can be found by examining the mutual interaction energy of particles in contact or close proximity.

Interparticle energies will always exist in granular media as a result of molecular and electrostatic potentials, as well as by chemical bonds. It is believed that short-range molecular potentials are primarily responsible for the behavior of compactable powders. It should be noted that these potentials are always present and the associated interparticle forces are always attractive.

The total energy per unit volume of a powder, owing to interparticle potentials of molecular origin, can be considered to be proportional to the number of particle contacts per unit volume. It is clear that the interparticle energy per unit volume increases rapidly with increasing powder bulk density (See Section 2.1.1.1). On the other hand, the gravitational potential energy increases with decreasing density. The equilibrium density of the powder corresponds to the condition of minimal total energy. This is illustrated in Figure 2.1.

---

[*] The basic distinction here is that dilatant materials cannot be sheared until the particles fracture, while compactable powders can be sheared with a small increase in applied load (e.g., in the piston-cylinder test).

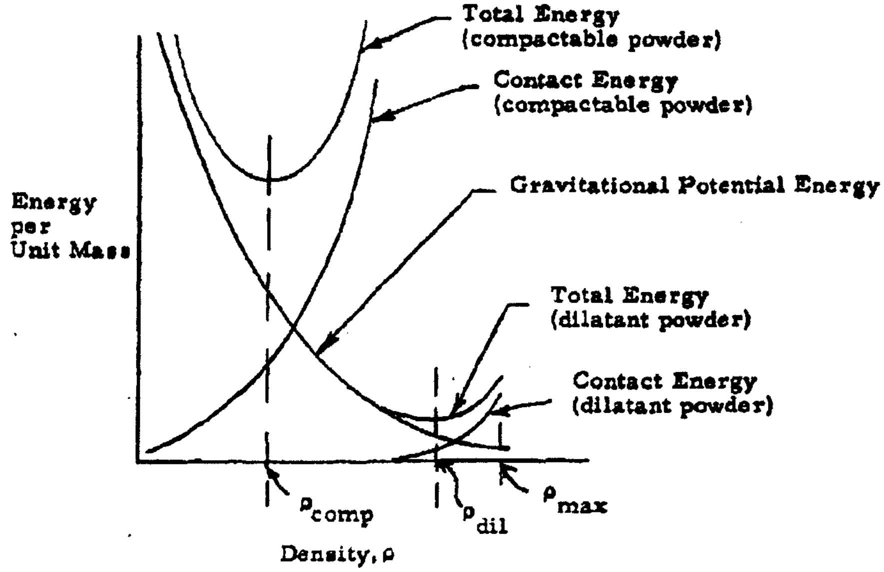

Figure 2.1. Energy Balance at Equilibrium for a Compactable Powder

As shown in the figure, the gravitational potential energy depends only on the powder density. However, the contact energy per unit mass depends markedly upon the particle size. For a typical dilatant powder, the number of contacts per unit mass is comparatively small; thus, the minimal total energy occurs at a density approaching the density of the solid material (for spheres, the maximum density for a close-packed array is $0.74\ \rho_p$, where ρ_p is the particle density). For compactable powders, the contact energy is so great that equilibrium is reached at a much lower density (note upper curve in Figure 2.1).

The dependence of contact energy on particle size can be seen by considering a hypothetical powder consisting of spherical particles of diameter d_p. The number of particles per unit mass is:

$$N = \frac{6}{\pi \rho_p d_p^3} \; . \tag{1}$$

The contact energy per unit mass can be expressed by the relationship:

$$E_c = N\epsilon f\left(\frac{\rho}{\rho_p}\right) = \left(\frac{6}{\pi \rho_p d_p^3}\right) \epsilon f\left(\frac{\rho}{\rho_p}\right) \tag{2}$$

E_c = (particles/unit mass)(av. energy/contact)(contacts/particle)

in which ϵ is the average energy per contact and $f(\rho)$ is a function giving the number of contacts per particle as a function of the average powder density ρ. It is easily seen that the function $f(\rho)$ satisfies the conditions: $1/2 \leq f(\rho/\rho_p) \leq 6$; $f^1(\rho/\rho_p) > 0$. (The condition $f(1) = 6$ corresponds to hexagonal packing; i.e., six contacts per particle.) According to Deriagin and Abrikosova [3], the energy ϵ is proportional to d_p. Thus, for spherical particles, the bulk contact energy varies inversely as d_p^2.

A mathematical analysis of the compaction function $f(\rho/\rho_p)$ for the special case of uniform spherical particles is given in Section 2.1.1.1. For particles of nonuniform size it is clear that the smaller particles may contribute greatly to the total energy even when constituting a small mass-fraction of the powder. The role of particle shape in the compaction process is very complex; however, elongated or platelet forms can be expected to result in reduced powder density and a tendency toward compactability (e.g., consider snowflakes or talc powder).

It has been tacitly assumed in the above discussion that the powder is initially deagglomerated; for example, the powder could be considered to settle out from an aerosol composed of discrete particles. It has also been assumed that the powder layer is very thin, since the weight of a thick powder layer causes progressive compaction within the layer. In actuality, most powders in a natural state consist of agglomerates which presumably result when the powder is repeatedly compacted and broken up during handling. There are indications that the handling properties of compactable powders are improved by agglomerates of this type. This is not surprising since the agglomerates can be regarded as large particles for which the "interagglomerate" energy is small relative to the average agglomerate mass.

2.1.1.1. Analytical Compaction Theory

A very simple theoretical model of the compaction process has been advanced by Derr[4]. This model yields a compaction stress-density relationship of the form:

$$\sigma = C\rho^{m}\left\{1 + \left(\frac{\rho_o}{\rho}\right)^{m}\right\} \tag{3}$$

and shows furthermore that the cohesive shear strength of a compacted powder is proportional to the compaction stress. (The last term in the brackets of Equation (3) is usually negligible compared with unity.) Both of these conclusions are in good agreement with experimental results.

Derr's theory is based on a particular agglomerate structure, i.e., the geometrical arrangement of the powder particles is specified for each density state. A different approach, based on energy considerations, is taken in the following analysis.

Energy of Compaction - We assume that the powder is composed of spherical particles of diameter d_p. Also, it is assumed that the energy of a single contact is ϵ. We wish to determine the energy required to produce a given change in the average powder density.

Suppose that a powder sample contains N particles. In an unstressed state the total contact energy is distributed among the N particles in accordance with the number of contacts per particle. It is apparent that a particle may have from 1 to 12 contacts with neighboring particles. If we assign half the total contact energy to each of the particles in contact, the energy state of a particle may range from $\epsilon/2$ to $12(\epsilon/2)$.

We now ask: For a given total contact energy E_c, how are the energy states distributed among the N particles? Let the total energy E_c be expressed in the form:

$$E_c = \sum_{1}^{12} E_i \tag{4}$$

where E_i is the energy due to particles with i contacts per particle.

It can be shown from the theory of statistical mechanics[5] that the number of particles in each energy state can be expressed by the distribution function:

$$N_i = NA(e^{-\alpha i \epsilon/2}) \tag{5}$$

where A and α are constants. Letting $x = e^{-\alpha \epsilon/2}$, the constant A is defined by:

$$N = \sum_{1}^{12} N_i = NA \sum_{1}^{12} x^i$$

or

$$A = \frac{\frac{1}{x} - 1}{1 - x^{12}} . \tag{6}$$

The total contact energy is:

$$E_c(x) = \frac{NA\epsilon}{2} \sum_{1}^{12} i\, x^i = \frac{N\epsilon}{2} \; \frac{1 + 12x^{13} - 13x^{12}}{(1 - x)(1 - x^{12})} \; . \tag{7}$$

The energy invested in i^{th} order contacts is:

$$E_i(x) = \frac{N\epsilon}{2} \; \frac{\frac{1}{x} - 1}{1 - x^{12}} \; i\, x^i \;\; (i = 1, 2, 3 \; . \; . \; . \; 12) \; . \tag{8}$$

A number of the energy functions $E_i(x)$ are plotted in Figure 2. 2. The energy parameter x is small for small values of total energy (i. e., for low powder density) and increases with increasing total energy. This parameter can also be related directly to the powder density as will be shown later.

The energy functions plotted in Figure 2. 2 give a very good picture of the essential features of the compaction process. At low densities (small x), most of the contact energy is distributed among the low energy states. As the density (and x) increases, the energy distribution shifts continuously toward states of higher energy.

It will be observed also that each energy state ($i = 2, 3 \ldots, 11$) increases from $E_i(o) = 0$ to a maximum value and then falls off to zero as x becomes infinite. For any value of the parameter x, Equation (7) gives the total contact energy. As x increases, however, the energy which must be supplied includes not only the incremental value of total contact energy but also the energy needed to break down lower energy states. The latter energy component evidently represents the effects of cohesion.

The total energy change during compaction, denoted by E(x) (relative to x = 0), is plotted versus x in Figure 2. 3. (The change in $E_1(x)$ was

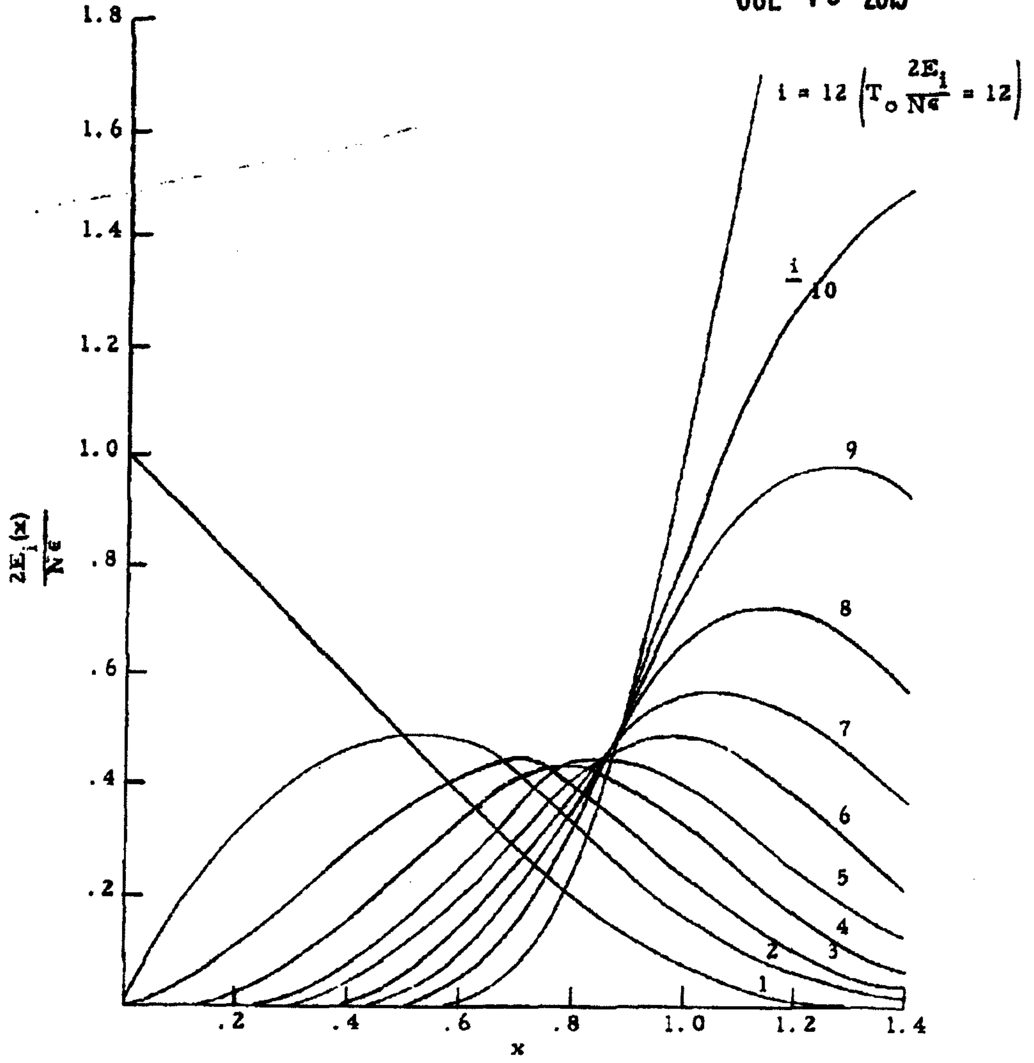

Figure 2.2. Contact Energy $E_i(x)$ vs. Compaction Parameter x

Page determined to be Unclassified
Reviewed Chief, RDD, WHS
IAW EO 13526, Section 3.5
Date: JUL 19 2013

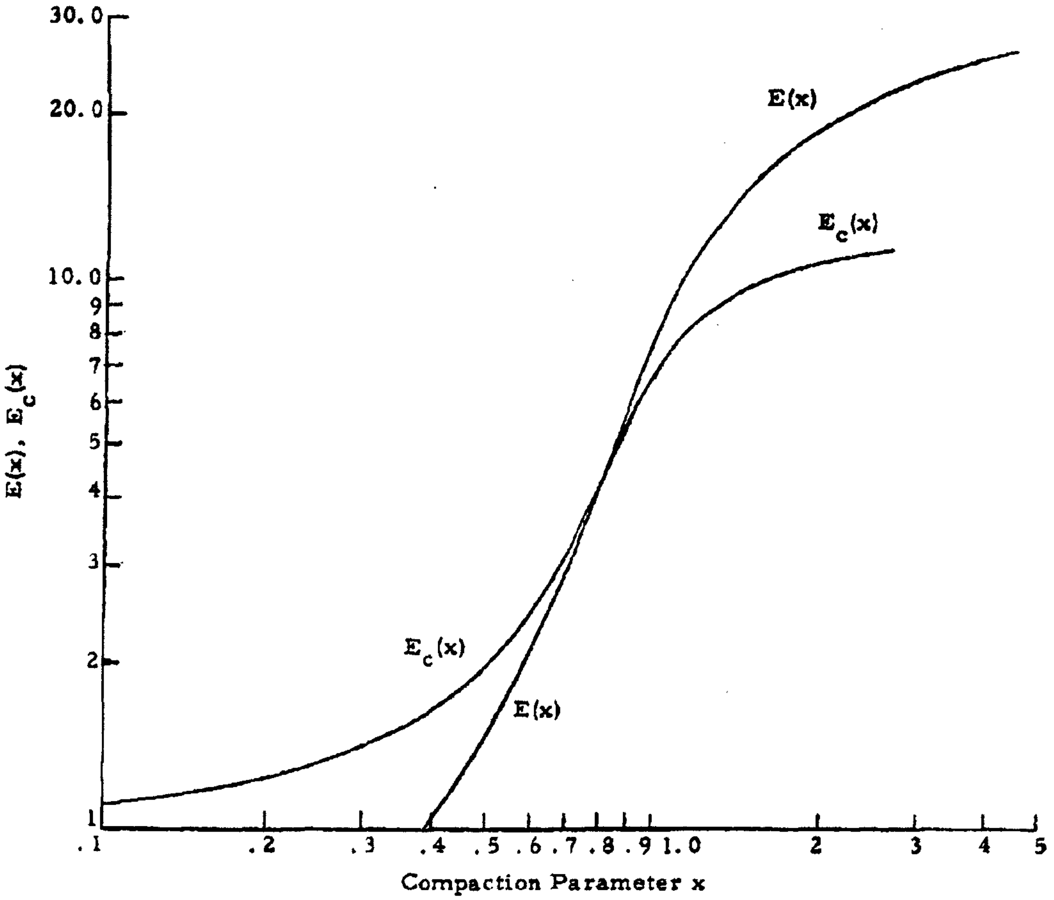

Figure 2.3. Contact Energy $E_c(x)$ and Compaction Energy E(x) vs. Compaction Parameter x

ignored in these calculations, since single contacts are physically improbable.) The contact energy $E_c(x)$ (from Equation 7) is also shown in Figure 2.3.

Relationship between Compaction Energy and Powder Density - The bulk density of the powder for a given compaction state can be determined in the following way. Equation (5) gives the fractional number of particles in each energy state in terms of the parameter x. For the i^{th} state:

$$N_i/N = \frac{\frac{1}{x} - 1}{1 - x^{12}} x^i = Ax^i. \tag{9}$$

Particles in the i^{th} energy state have i contacts with neighboring particles. Denote the volume occupied per particle in the i^{th} energy state by $a_i v_p$, where $v_p = \frac{\pi}{6} d_p^3$ is the particle volume. The total volume for N particles is:

$$V(x) = v_p \frac{\frac{1}{x} - 1}{1 - x^{12}} \sum_1^{12} a_i x^i . \tag{10a}$$

The bulk density is then:

$$\rho(x) = \frac{N \rho_p v_p}{V(x)} = \rho_p \frac{x - x^{13}}{(1 - x) \sum_1^{12} a_i x^i} . \tag{10b}$$

For the close-packed state (i = 12):

$$a_{12} = \frac{6}{\pi} \cos \frac{\pi}{6} \sqrt{1 - \tan^2 \frac{\pi}{6}} = 1.35 .$$

Similarly, for square packing (i = 6): $a_6 = \frac{6}{\pi} = 1.91$ and for hex-packed layers stacked one above another (i = 8): $a_8 = \frac{6}{\pi} \cos \frac{\pi}{6} = 1.65$. The latter arrangements are the most loosely packed arrays corresponding to i = 6 and i = 8, respectively. The densest packings for i = 6 and i = 8 are nearly hexagonal arrays, slightly displaced to open six contacts (i = 6) or four contacts (i = 8). On the average, therefore, we have:

$$a_6 = \frac{1}{2}(1.35 + 1.91) = 1.63 \text{ and } a_8 = \frac{1}{2}(1.35 + 1.65) = 1.50 .$$

These values are plotted vs. the number of contacts i in Figure 2.4; since they lie on a linear log-log curve, it is assumed that the a_i values can be read from the figure for other values of i. These values are given in the following table.

i	1	2	3	4	5	6	7	8	9	10	11	12
a_i	2.65	2.20	1.97	1.82	1.71	1.62	1.56	1.51	1.47	1.42	1.38	1.35

By computing the compaction energy and the bulk density as functions of x, an implicit relationship may be established between compaction energy and bulk density. The results of these calculations are shown in Figure 2.5. The dimensionless compaction energy $2E/N\epsilon$ is plotted vs. the density ratio ρ/ρ_p. If E is interpreted as the energy per unit mass, the ordinate in Figure 2.5 can be expressed as:

$$\frac{\pi \rho_p d_p^3 E}{3\epsilon} .$$

Thus, the energy for a given density varies directly as (ϵ/d_p^3).

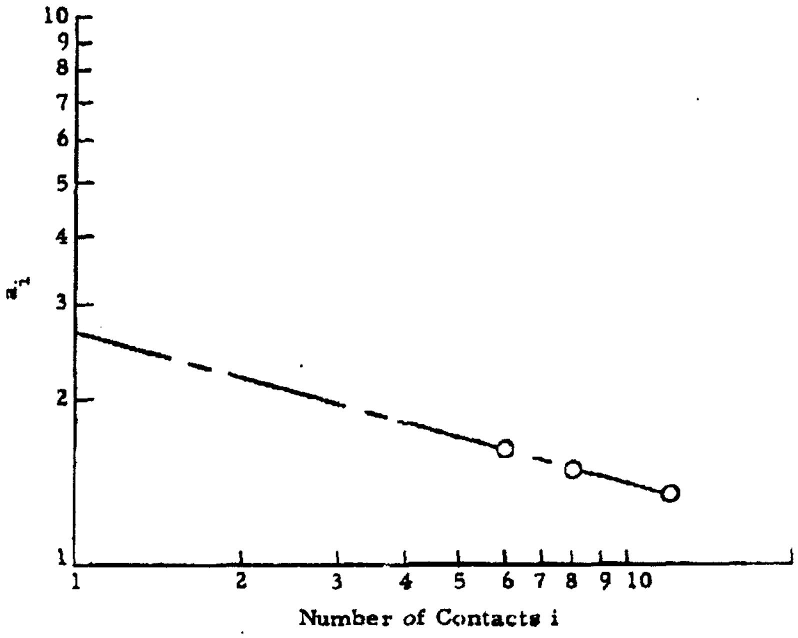

Figure 2.4. Volume Coefficients a_i vs. the Number of Contacts per Particle i

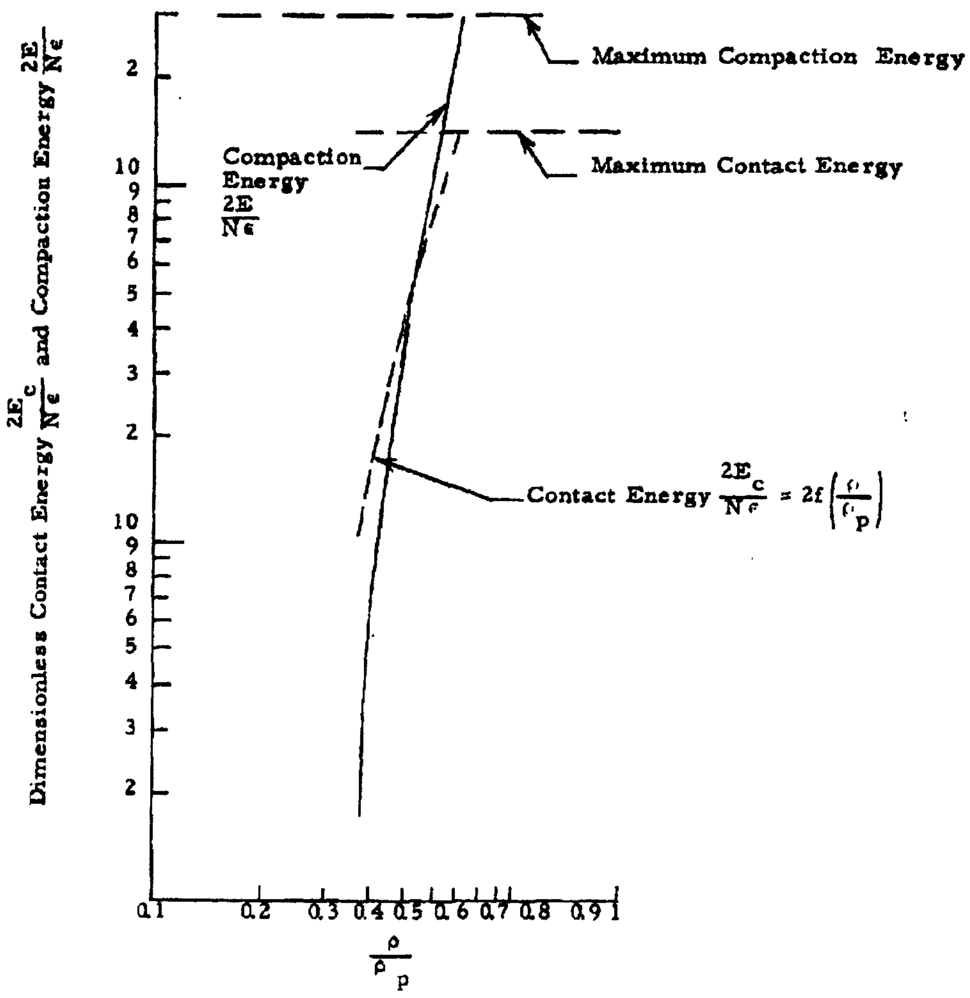

Figure 2.5. Theoretical Compaction and Contact Energies vs. Density - Spherical Particles

Over most of the density range the compaction energy is closely approximated by the equation:

$$E = 151 \frac{\epsilon}{\rho_p d_p^3} \left(\frac{\rho}{\rho_p}\right)^{5.67} . \tag{11}$$

The dimensionless contact energy function $f\left(\frac{\rho}{\rho_p}\right) = \frac{E_c}{N\epsilon}$ is also plotted in Figure 2.5.

Compaction Stress as a Function of Density - The compressive stress required for compaction can be found from the compaction energy by equating the work done by the compaction stress to the change in energy between density states ρ_1 and $\rho_2 > \rho_1$. Consider a unit mass of powder, contained in a smooth-walled cylinder of cross-sectional area A. If x is the depth of the powder, $\rho Ax = 1.0$. Now, if the powder is compacted with a smooth piston, we have:

$$\sigma\, A dx = -dE$$

or

$$\sigma = \rho^2 \frac{dE}{d\rho}$$

$$= \frac{855\, \epsilon}{d_p^3} \left(\frac{\rho}{\rho_p}\right)^{6.67} . \tag{12}$$

The theoretical compaction relationships shown in Figure 2.5 and expressed by Equations (11) and (12) are very similar to experimentally determined compaction characteristics. Both the theoretical and experimental results show a very rapid increase in compaction energy (or applied stress) with increasing bulk density. This characteristic strongly implies that short-range interparticle potentials have a dominant influence on the compaction process. The theory also indicates that the compaction energy increases rapidly with decreasing particle diameter. For particles in the micron size range, the contact energy-size relationship is expected to lie somewhere between an inverse second or inverse third-power law. It follows from this that the behavior of powders is determined largely by the smallest particles in the particle size distribution.

2.1.1.2. General Behavior of Compactable Powders

During our study of the behavior of dry powders several theoretical and empirical laws have been advanced to describe the compaction characteristics of dry powders. These laws may be stated as follows:

1) The compressive stress required to compact a powder to a density ρ can be expressed by an equation of the form:

$$\sigma = k\rho^m \tag{13}$$

where k and m are constants for a given powder.[6]

2) The shear resistance τ_c of a powder undergoing compaction is proportional to the applied normal (compressive) stress on the shear plane, σ_n:

$$\tau_c - \tau_o = \sigma_n \tan \phi \tag{14}$$

The angle ϕ is a constant for a given powder; τ_o is the shear resistance of the powder in an uncompacted state.

3) The shear strength of a compacted powder can be described by the equation:

$$\tau = \sigma_n \tan \phi' + b\rho^m . \tag{15}$$

The first term on the right-hand side of this equation can be regarded as an effective "frictional" resistance, while the second describes the effect of cohesion on the shear strength.

The constants k and m may be found from the Instron compaction tests;[6] the constants ϕ' and ϕ are obtained from direct shear tests.[7] The constant b is derived from the constants A, ϕ and ϕ' in the following way. Referring to Figure 2.6, the cohesive shear component τ_{coh} is seen to be:

$$\tau_{coh} = \sigma_n (\tan \phi - \tan \phi'). \tag{16}$$

To define b, we must express σ_n in terms of the density ρ. The principal compaction stress corresponding to σ_n is $\sigma_{max} = \sigma_n \sec \phi$ (see Figure 2.6). The stress σ_{max} is related to the density through Equation (11). Therefore, from Equation (16):

$$\tau_{coh} = b\rho^m = A \cos \phi \, (\tan \phi - \tan \phi')\rho^m$$

or

$$b = A \cos \phi \, (\tan \phi - \tan \phi'). \tag{17}$$

The constant b is a measure of the effects of cohesion. A large value of b implies that a powder will be difficult to deagglomerate after compaction. If b is small a powder will generally be easy to deagglomerate. For dilatant media, $b \approx 0$ since $\phi \approx \phi'$.

Aerodynamic Breakup of a Compacted Powder - The deagglomeration of compacted *Sm* powder by aerodynamic forces has been intensively studied during this program by subsonic wind tunnel tests.[7] The above analysis provides a basis for estimating the effectiveness of aerodynamic breakup for different lots of *Sm* and for other powders. Suppose that a small agglomerate of compacted powder is suddenly injected into an airstream at a relative velocity U. This results in both shear and pressure stresses being applied to the agglomerate. The shear stresses are proportional to $U^{3/2}$ for laminar

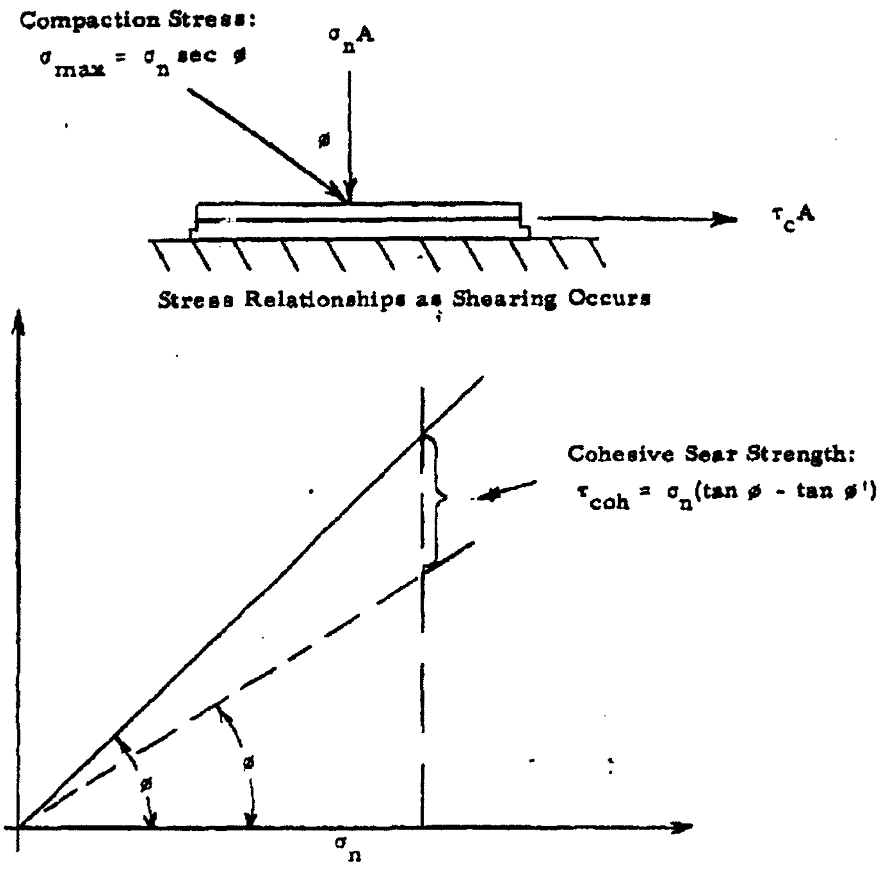

Figure 2.6. Analysis of Cohesive Shear Strength - Direct Shear Test

flow while the pressure stresses are proportional to the dynamic pressure $q = \frac{1}{2} \rho_a U^2$ (ρ_a denotes the air density). These stresses are resisted by the cohesive shear strength of the agglomerate, expressed by Equation (17). At the point of breakup, the relationship between critical velocity and powder density is:

For shear-induced breakup

$$U_{crit} = C_1 b^{2/3} \rho^{\frac{2m}{3}} \tag{18a}$$

For pressure-induced breakup

$$U_{crit} = C_2 b^{1/2} \rho^{\frac{m}{2}} . \tag{18b}$$

The constants C_1 and C_2 cannot be evaluated analytically for agglomerates of arbitrary shape. However, the above equations indicate how the critical speed varies with density for the two breakup mechanisms. The critical velocities for shear and pressure-induced breakup are plotted vs. density in Figure 2.7 for Sm 342 to illustrate Equations (18a) and (18b). The critical velocities are referred to the critical velocity at $\rho = 0.4$, the primary purpose here being to show the shape of the curves. In each case, the rapid increase in critical speed with increasing density closely resembles the experimental curve for Sm 342 (Figure 6.3, Reference 7).

The theoretical critical speeds for Sm 352 as compared with Sm 342 have been computed as a function of density by using Equation (18b) (assuming pressure-induced breakup) and Equation (15). Using data from the Thirteenth Quarterly Report,[8] the following constants are found for the two Sm lots:

Lot	ϕ	ϕ'	m	A	b
342	40.6°	37.0°	14.5	1.53×10^{10}	1.24×10^{9}
352	42.5	39.2	11.6	2.04×10^{9}	1.52×10^{8}

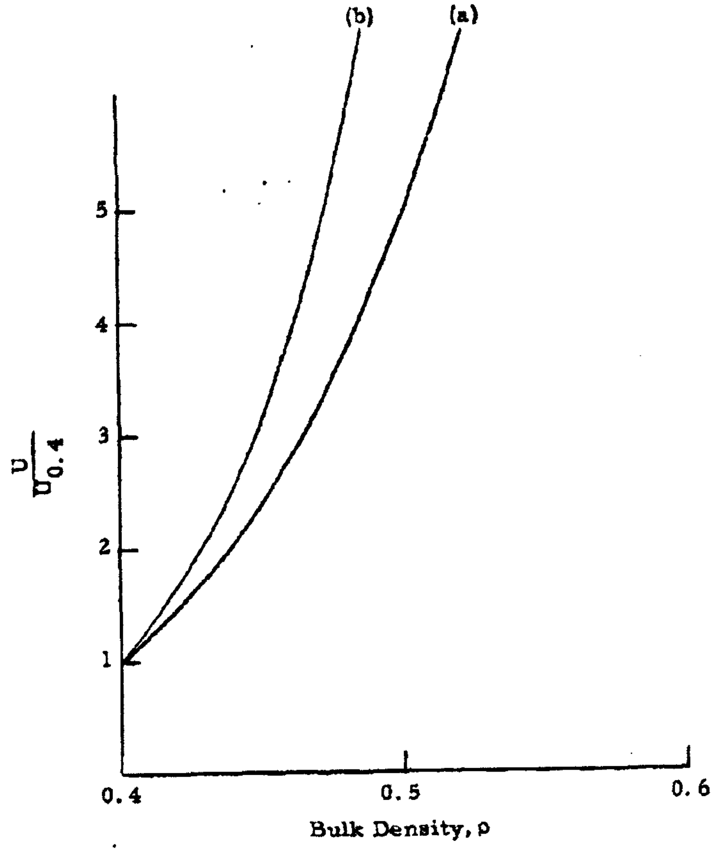

Figure 2.7. Theoretical Aerodynamic Breakup of Sm 342 for: (a) Pressure-Induced Breakup, (b) Shear-Induced Breakup - Critical Speed vs. Density (Critical Speeds Relative to Critical Speed at ρ = 0.4)

The critical speed as a function of density for these Sm samples is plotted in Figure 2.8, taking the critical speed for lot 342 at $\rho = 0.4$ as unity. At the same density, there is a very significant difference in critical speed for the two Sm lots (this difference would be even greater for shear-induced breakup) at the same density. If the two lots are compared at the same compaction stress, however, the critical breakup velocities are not greatly different.

2.1.1.3. Behavior of Compactable Powders at Low Densities

The preceding discussion has been concerned primarily with the behavior of powders that have been compacted to an appreciable degree. It is noteworthy that the phenomena responsible for compactability also exert a strong influence on the behavior of "uncompacted" powders, i.e., powders which have not been deliberately or knowingly compacted. (Considerable compaction may occur by the weight of even a thin layer of powder.) Electrostatic or molecular interparticle forces may often exceed the mass of individual particles, leading to very high local angles of repose.

The behavior of powders under these conditions can be visualized in terms of the generalized shear strength relationship expressed by Equation (14). This equation is plotted in Figure 2.9 for small values of σ_n. The key factor in this equation, as far as uncompacted powders is concerned, is the initial shear strength τ_o. This is the shear strength of the powder in its "natural" density state. When a powder is compacted τ_o is usually negligible compared with the compaction shear strength τ_c. However, for an uncompacted powder this term may be large relative to the weight of the powder itself. This is illustrated by the following analysis.

Consider a uniform layer of powder of mass m_1 grams/cm^2 resting on a rough plane surface which is initially horizontal (see Figure 2.9). Owing to the weight of the powder (in this case very small) the powder layer will be slightly compacted. The corresponding shear strength characteristic

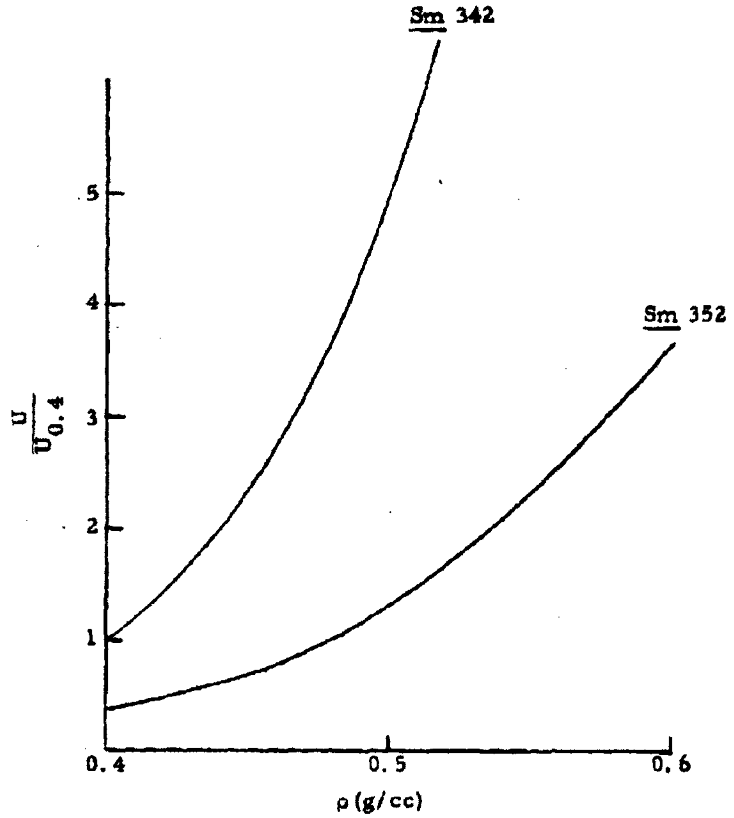

Figure 2.8. Theoretical Aerodynamic Breakup of Two Sm Lots - Critical Speed vs. Density (Critical Speeds Relative to Lot 342 at ρ = 0.4)

Page determined to be Unclassified
Reviewed Chief, RDD, WHS
IAW EO 13526, Section 3.5
Date: JUL 19 2013

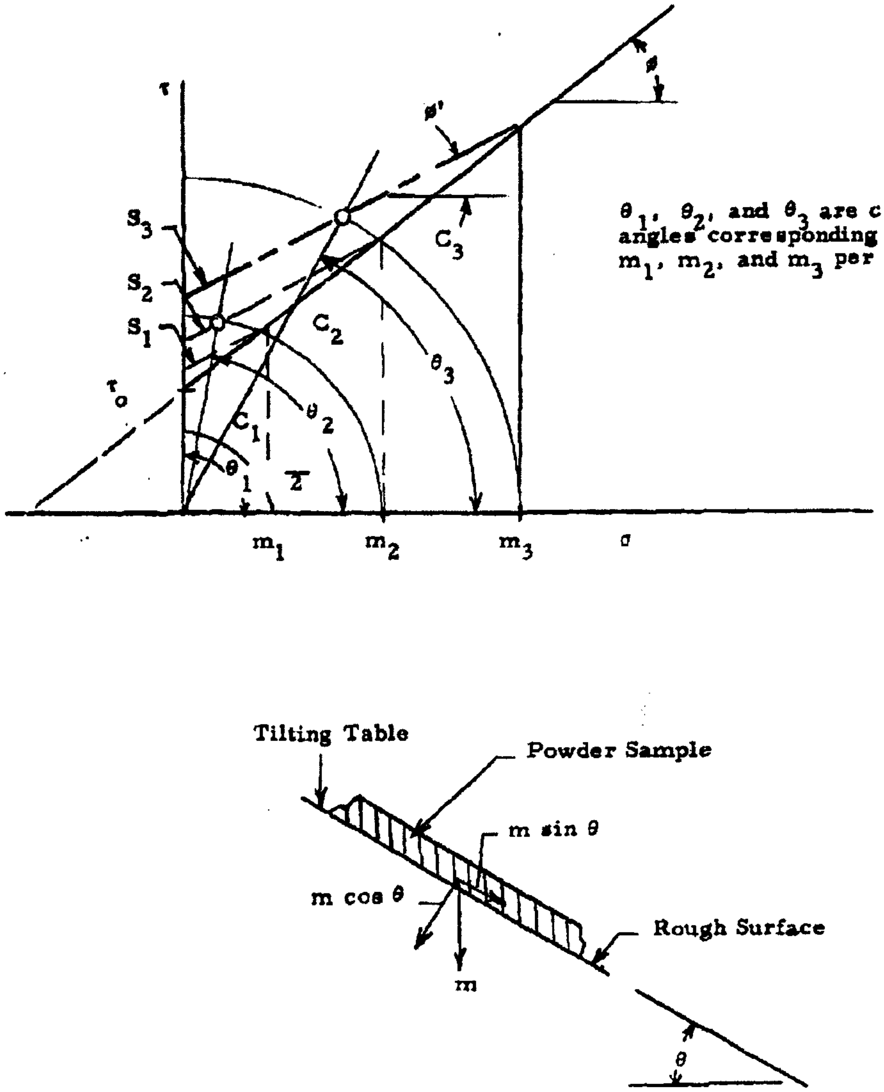

θ_1, θ_2, and θ_3 are critical angles corresponding to masses m_1, m_2, and m_3 per unit area

Figure 2.9. Critical Slide Angle Analysis

(including the effects of compaction due to the powder weight) is given by the line S_1 in Figure 2.9. Now suppose the surface is tilted through an angle θ; the shear stress at the surface is $m_1 \sin \theta$ while the normal stress is $m_1 \cos \theta$. The locus of applied stresses is thus a circle C_1 in the stress plot . For the condition shown, the powder layer will not slide off even at $\theta = 90°$. (This implies that the <u>local</u> angle of repose can exceed 90° for this layer.) If we now repeat this process for masses $m_3 > m_2 > m_1$, a series of critical slide angles will be obtained as indicated in Figure 2.9. If m is large, the slide angle is approximately equal to the shear angle ϕ . For decreasing mass densities, however, the slide angle progressively increases. This effect is frequently observed with granular or powdered materials. In particular, local angles of repose may exceed 90° for materials having an average angle of repose of 40 to 50°. Such behavior is observed in an extreme form under humid conditions. In a dry environment, electrification of powders caused by handling (i.e., by relative motion of powder particles and of the powder relative to the container) markedly affects many powders. Even dry dilatant materials can exhibit cohesion under certain conditions (e.g., marked cohesion effects have been observed for magnetized steel shot, having angles of repose exceeding 90°).

Of course, the intercept τ_o cannot be considered a constant for a given powder; rather, it is a statistical parameter which depends on the history of a powder sample. The general trend of increasing <u>mean</u> angle of repose with decreasing powder mass is likely to be found for most powders with MMD values in the micron size range. If the tests described above were performed many times for a given powder, it is probable that a great deal of scatter would be observed for small values of the powder mass per unit area m; however, the scatter would tend to decrease with increasing m.

2.1.2. Current Studies with Bg and Agent LX

2.1.2.1. Compaction Characteristics

Since Bg lot SCH-63-109 is to be used in forthcoming flight tests, a representative sample of this material was studied in comparison with Bg lot 17 used previously, so that realistic test parameters for compaction and dissemination could be predicted. The comparative stress density relationships shown in Figure 2.10 indicates that lot SCH-63-109 is somewhat more difficult to compact than the lot 17.

Figure 2.11 includes the stress density relationship for Bg lot SCH-63-109, lot 17, and agent LX in comparison with other powders studied recently. Clearly, the generalization that increased ease of compaction with increasing particle size does not apply. The egg embryo and agent LX have the largest MMD but are far more difficult to compact. These materials, in contrast to the other powders shown in Figure 2.11, are highly elastic and highly irregular in shape (Section 3, electronmicrographs). The relationship between ease of elasticity and ease of compaction will be studied in detail in the coming months.

2.1.2.2. Shear Strength and Tensile Strength of Agent LX

Like the highly elastic powders talc and egg embryo, the tensile strength of agent LX is also too low to measure by the segmented column method. Figure 2.12 shows the compaction shear strength of agent LX in comparison with egg embryo. The higher compaction shear strength for agent LX is consistent with the compaction data, indicating increased difficulty to compact.

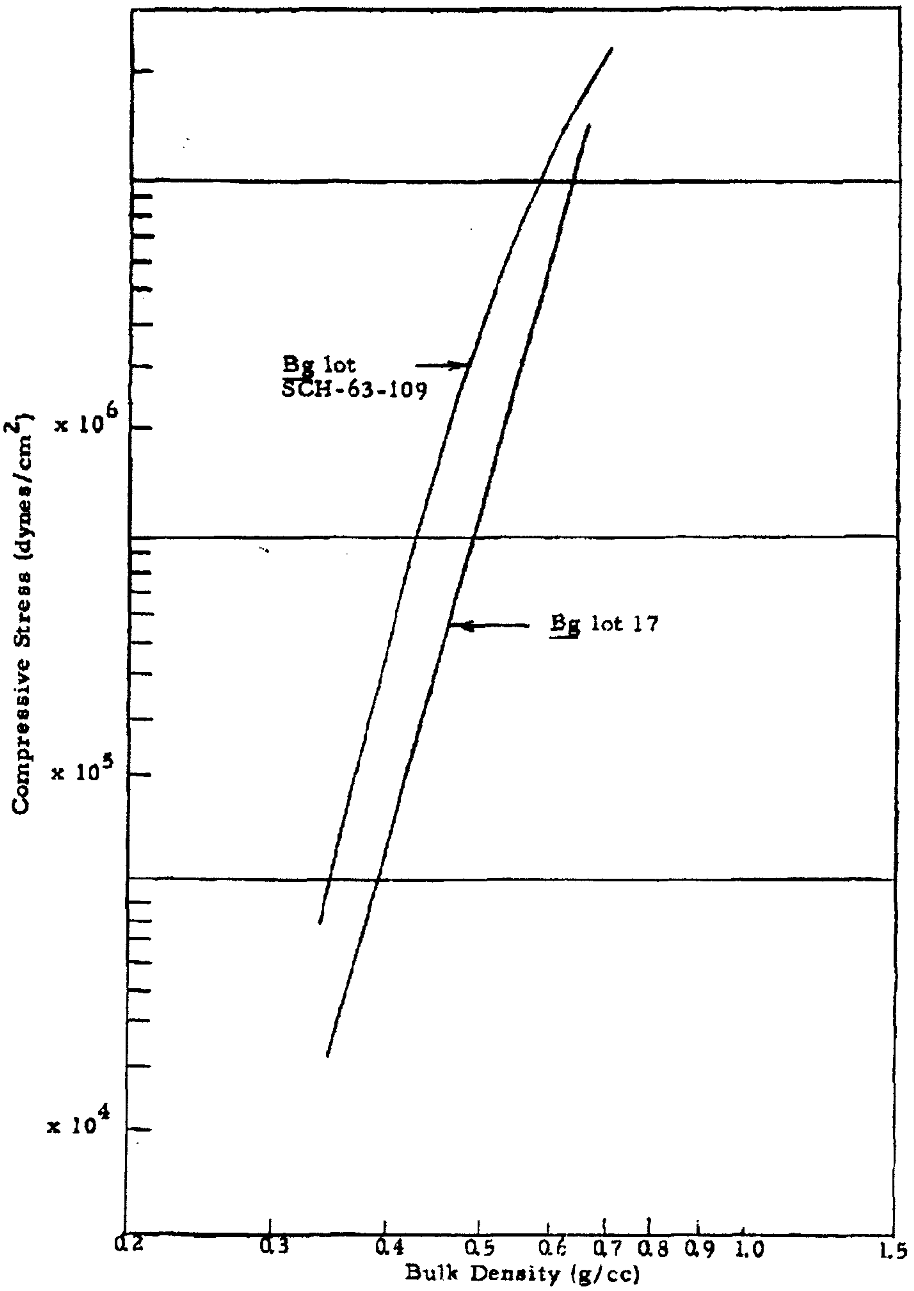

Figure 2. 10. Compaction Characteristics of Bg

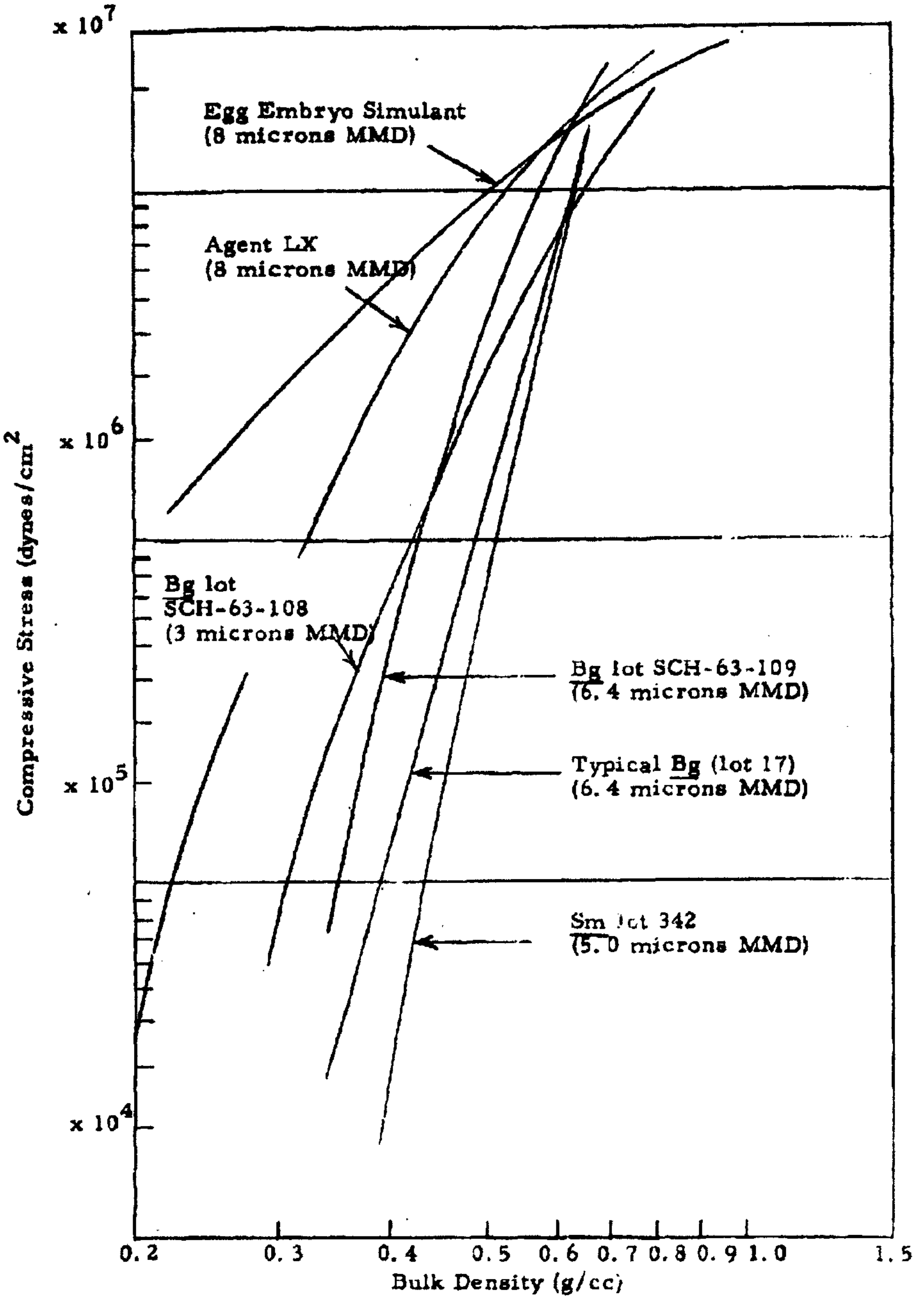

Figure 2.11. Compaction Characteristics of Powders

2.1.3. Analysis of Instron Compaction Data

At present, much data exist for many powders on compressive stress as a function of density. If the data were presented in terms of energy per unit mass rather than compressive stress, one would have more useful correlations.

The energy per unit mass can readily be obtained as a function of density if, for the powder in question, a plot of the logarithm of compressive stress versus density yields a straight line (this is usually the case for stress levels below 10^7 dynes/cm). Then the empirical equation

$$\sigma = k \rho^m \tag{19}$$

where σ = compressive stress

k = constant of the powder

ρ = bulk density

m = constant of powder, = the slope of the line on a plot of $\log \sigma$ vs. ρ.

can accurately be fitted to the data.

Because the compaction apparatus shown in Figure 2.12 of the Ninth Quarterly Progress Report has always been used with the Instron to obtain compaction data, it is possible to express the density (ρ) as a function of the distance traveled by the compacting piston (X) using the following relation:

$$\rho = \rho_o \frac{L}{L-X} \tag{20}$$

where ρ_o = initial bulk density

L = depth of powder receptacle.

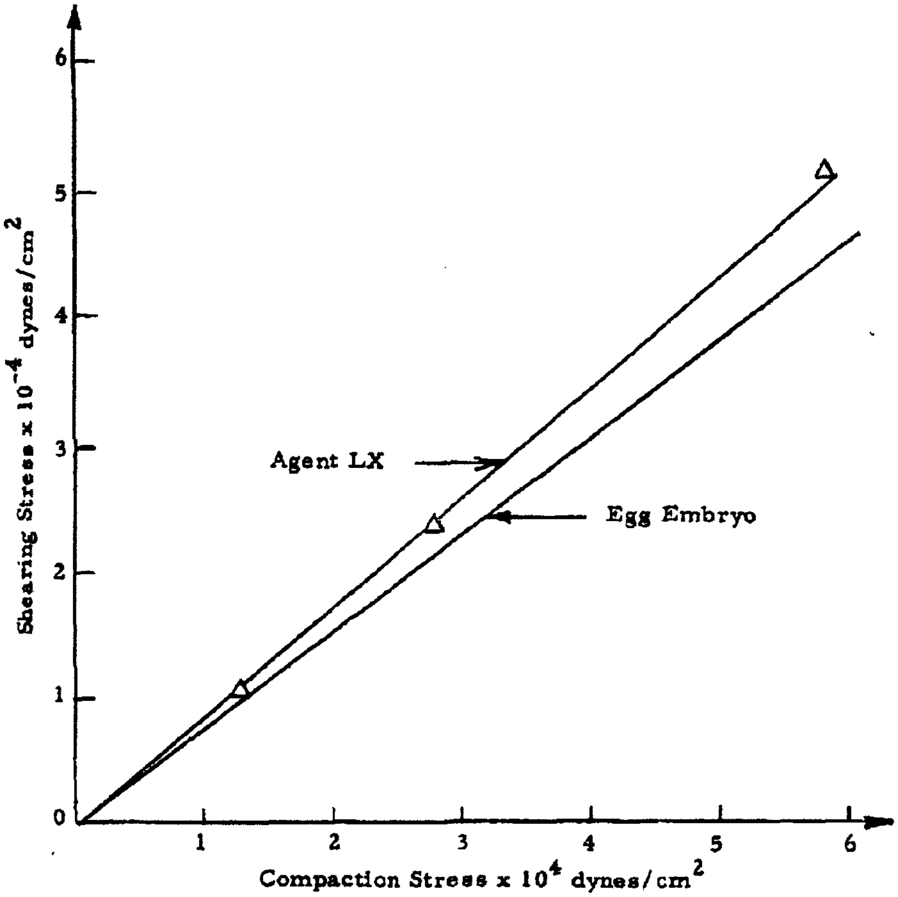

Figure 2.12. Compaction Shear Strength

The two above equations can be combined and integrated to yield a useful expression in energy (E) per gram (g), namely,

$$E/g = \frac{k}{(m-1)} \left(\rho^{m-1} - \rho_o^{m-1}\right). \qquad (21)$$

The energy of compaction of Bg product lot SCH-63-109 is shown in Figure 2.13 as measured from the data by a plainmeter and as calculated from Equation (3), using $k = 1.9 \times 10^9$ and $m = 9.01$. The constants k and m were determined from Figure 2.10.

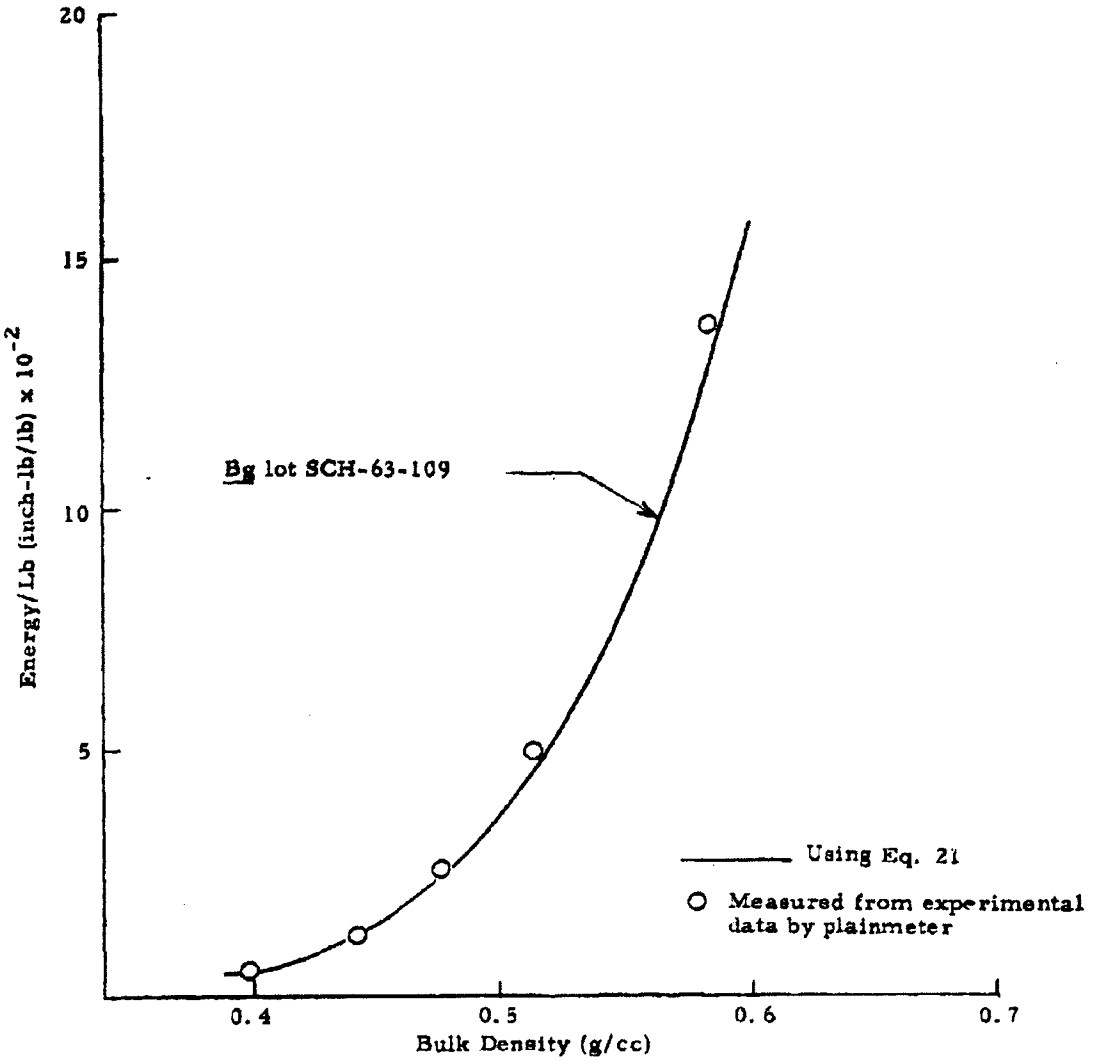

Figure 2.13. Energy of Compaction of Bg Lot SCH-63-109

3. PHYSICAL AND CHEMICAL CHARACTERISTICS OF THE POWDER PARTICLE

3.1. Total Surface Area

Surface areas for egg embryo, agent LX, and spray-dried saccharin were measured by the BET adsorption technique. The scatter of points in the BET plots as well as in the adsorption isotherms suggested the possibility of a systematic error of random magnitude. This problem was investigated during this last quarter through a study of buoyant forces. It is of considerable importance to maximize the accuracy of this technique since we hope to measure small changes in surface area (as a barometer of particle fracture during compaction) and other manifestations of change in surface structure of particles.

3.1.1. Study of Buoyant Force Correction

For larger surface areas the correction due to buoyancy is not significant. However, as the surface area decreases (hence, the amount adsorbed decreases) this correction assumes increasing importance. In this study the buoyancy correction has been only for the quartz bucket and fiber that have been below the level of the liquid nitrogen bath. The additional buoyancy of the spring was measured experimentally with no load in the quartz bucket. At the same time the magnitude of the experimental errors estimated and some sources of these errors were located.

The experimental data of buoyant force as a function of pressure are plotted in Figure 3.1. The lines are straight since buoyant force is a linear function of pressure, but the disturbing feature is that the lines did not pass through zero but fell in a band 0.1 mg wide (with an average intercept of 0.1 mg). No line passed through zero, or below, as might be expected from random error, indicating the existence of a systematic error of random

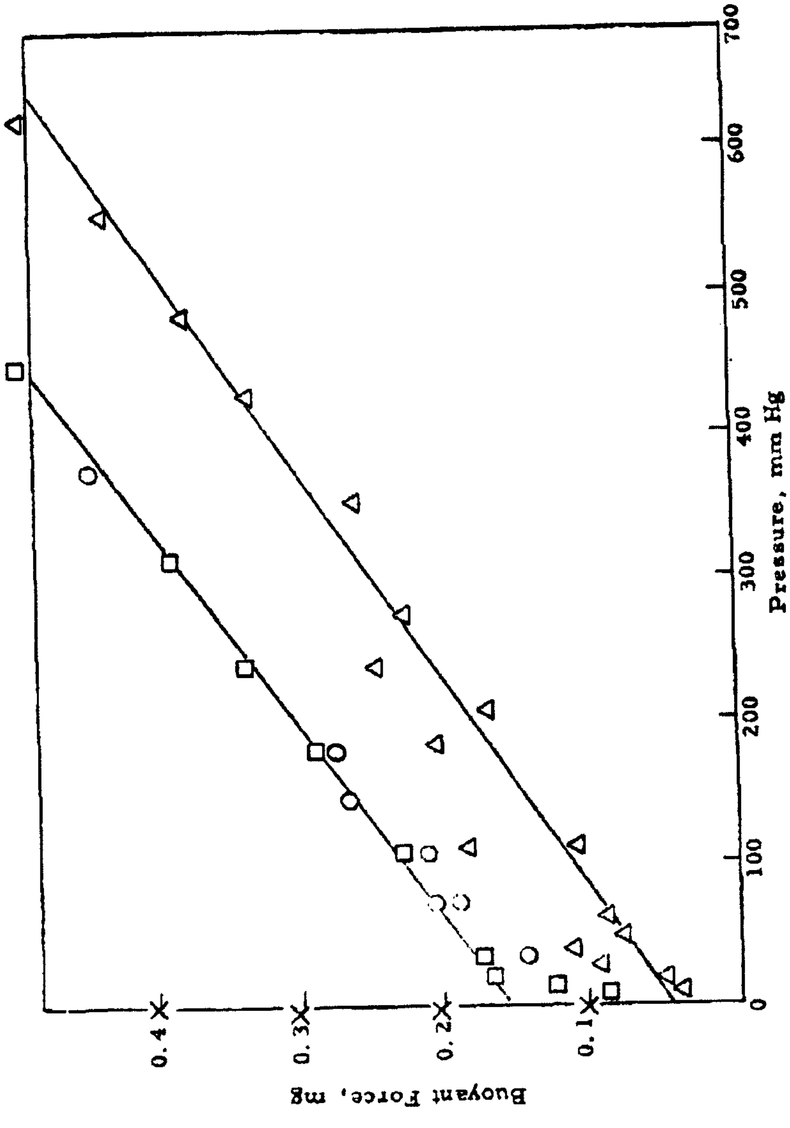

Figure 3.1. Buoyant Force as a Function of Pressure for the Quartz Spring, Bucket, and Fibers of Adsorption System

magnitude of 0.1 mg ±0.05 mg. The source of this error was found to be from lifting of the apparatus as the cover of the liquid N_2 dewar was snugged against the clamp holding the sample bulb. The clamp was used as a reference so that the level of the liquid N_2 would be the same in each run. If we avoided touching the clamp with the dewar cover, the points to cluster were lowered to about an intercept of 0.05 mg (corresponding to movement of approximately 0.04 mm). A reference point would be desirable but experimental difficulties of placing a reference point in the field of vision are great. Therefore the correction starts not from zero but from approximately 0.05 mg (Figure 3.2).

As an example, the effect of the correction and the effect of the errors on the data for Sm 352 presented last quarter[8] will be shown. Using the results from the error analysis[7] the additional error in the experimental determination of buoyant force was added to the rest of the errors.

For the correction of the BET data collected, the buoyant force data shown in Figure 3.2 will have an additional correction for the systematic error of 0.05 mg. The error is also assumed to be the range of the experimental data in Figure 3.1 or ±0.05 mg. This will be added to the errors in the manner outlined before[7], or the error in the buoyant force is:

$$dW'_{Bf} = \left[\left(\rho_g V_s \frac{d\rho_s}{\rho_s}\right)^2 + (dC)^2\right]^{1/2} . \qquad (22)$$

The first term is the error in the buoyant force on the sample, the second being the experimental error, .05 mg.

The new adsorption data are presented in Figure 3.3 along with the normal error bars. The area increases from 3.14 ±5 percent to 3.76 m^2/g ±3.7 percent. Although there is an area increase, the deviation determined before was actually taking into account the systematic error. The previous data on surface area measurements will be corrected in a similar manner.

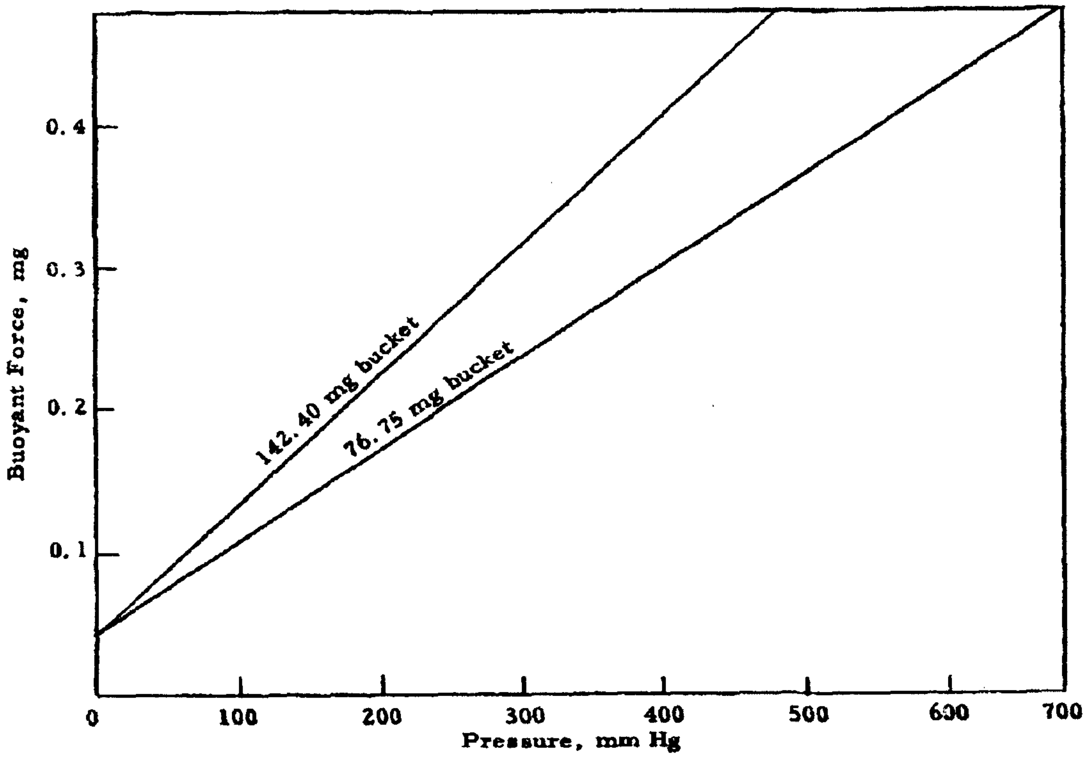

Figure 3.2. Buoyant Force on Quartz Spring, Bucket, and Fiber as a Function of Pressure and Weight of Bucket

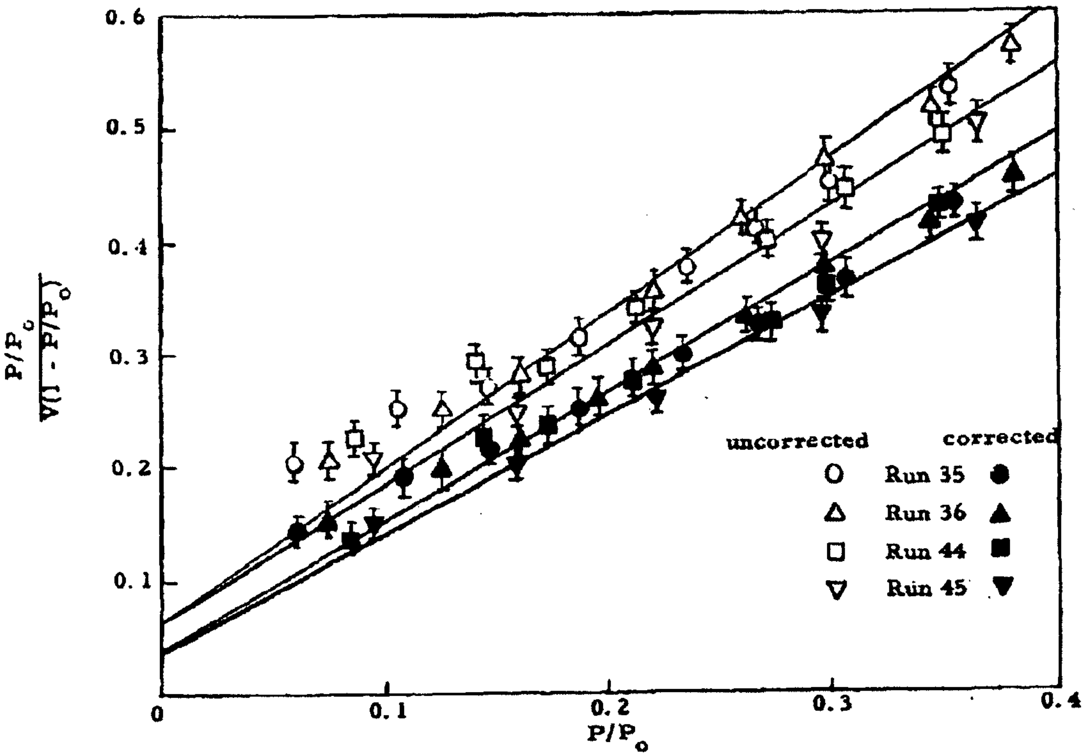

Figure 3.3. BET Plot of N_2 Adsorption on Sm 352 Showing Effect of Correction on Data

The changes in procedure necessary to eliminate the aforementioned systematic errors and the experimentally determined buoyant force on the quartz components should improve the accuracy of the data. As has been noticed before, the data for each individual run have much less deviation than deviation between duplicate runs. We hope to have corrected this now to enable us to better evaluate smaller changes in surface more reliably. However, it must be mentioned that the gravimetric system is best suited for particles under 5 to 7 microns because, in this range, buoyant forces are as large as the weight adsorbed. Over this range, what is actually measured is the difference between the calculated buoyant force and the observed buoyant force; if the buoyant forces can be accurately predicted this should pose no problem. The measurement of the total surface areas of the larger particle size powders or small changes in surface area is best suited to a volumetric system, the only advantage being that the buoyant force is eliminated and replaced by the dead space determination in the sample bulb. The calculation is a bit more reliable for small surface areas.

3.1.2. Spray-Dried Saccharin, Egg Embryo, and Agent LX

To determine the upper limits of the BET gravimeter adsorption method, the total surface areas of two lots of spray-dried saccharin, 13C and 13D, were measured. These powders had a large Whitby MMD (13C was 8.85 microns and 13D was 11 microns) which made measurement of the area difficult and the uncertainties great. The measured total surface for 13C was 0.78 m^2/g ±40 percent and for 13D was 1.06 m^2/g ±22 percent. Rugosities were 2.0 for 13C and 2.2 for 13D.

Figures 3.4 and 3.5 show the BET plot of the data. As is obvious the error bars are extremely large, but in Figure 3.5 the error bars are shown to be not unrealistic since they span the range of points. In the previous section (3.1.1) it was pointed out that the major error is the error in the experimental determination of the buoyant force.

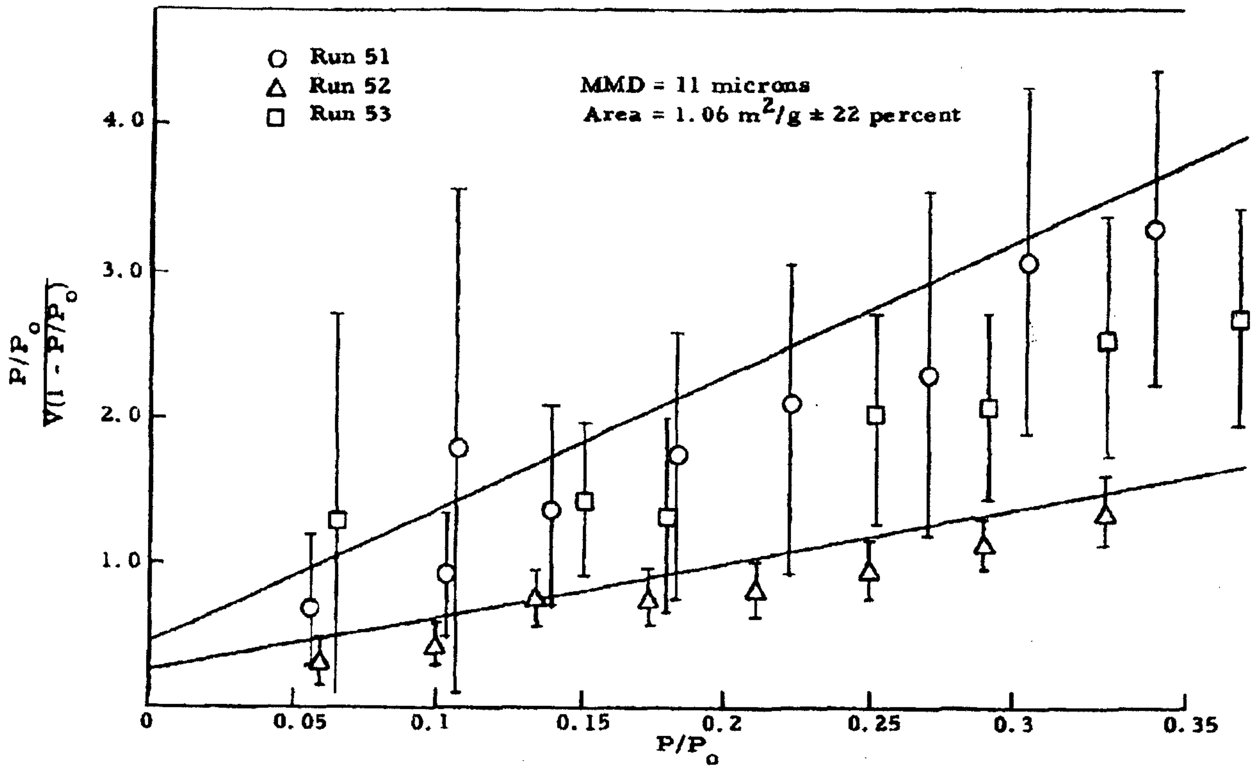

Figure 3.4. BET Plot of N_2 Adsorption on Spray-Dried Saccharin (13D) Showing Normal Error

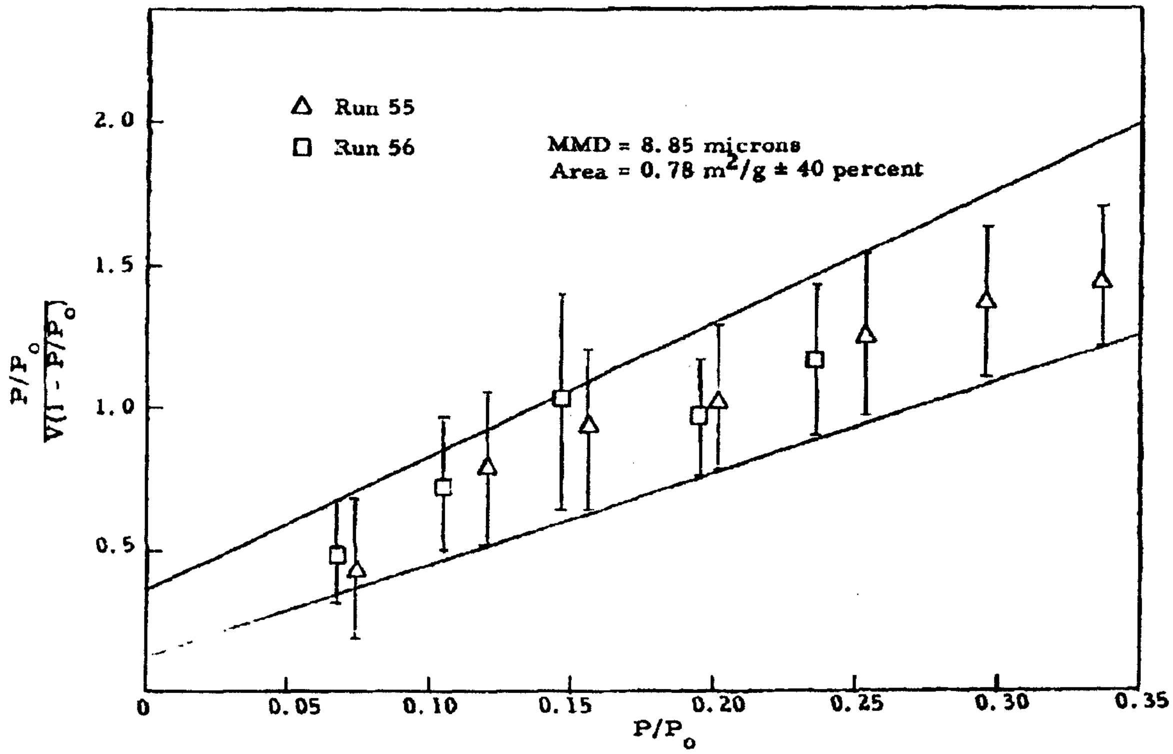

Figure 3.5. BET Plot of N_2 Adsorption on Spray-Dried Saccharin (13C) Showing Normal Error

This method can thus be used for approximating the surface areas for powders normally considered beyond the upper limits (5 to 7 microns) for the method.

In addition to the smooth spherical particles of spray-dried saccharin, two materials of radically different particle shape were studied. The surface areas of the agent LX, Figures 3.6 and 3.7, and egg embryo, Figures 3.8 and 3.9, were found to be quite large as were their rugosities. Surface areas of the agent LX were 4.40 m^2/g ±4 percent and for egg embryo, 14.2 m^2/g ±7 percent. Their rugosities were 6.8 and 26.8, respectively.

The large rugosity of egg embryo is in the same range as talc[9]. The difference between the two is that talc has a small particle size, approximately 1.75 to 3.5 microns, while egg embryo is large, approximately 8 microns. The high rugosity of talc results from its being a very irregular platelet structure and possibly having some macropore structure. Egg embryo, on the other hand, is a mixture of particles of widely varying size, shape, and constitution; here, also there is the possibility of some macropore structure because of the steep rise of the curve as $P/P_o \rightarrow 1$. There is negligible hysteresis in the adsorption-desorption isotherm (Figure 3.9). However, if the silica in egg embryo is of the porous type, a few pores could be left open which would have little volumetric effect but augment the surface area. The extent of such structure is small indeed(if the structure exists at all) since the surface area is still quite small as compared to a truly porous material.

A characteristic shared by both talc and egg embryo is greater elasticity at low bulk density--a characteristic shared also by agent LX, whose rugosity is much lower than either talc or egg embryo. In all three cases the particle shapes are very irregular, indicating that particle shape may determine the extent of elasticity. A large rugosity (greater than 6) with the absence of extensive pore structure, seems to indicate that there will be much elasticity. The relationship between rugosity and elasticity--particularly for highly elastic materials--will continue to be investigated.

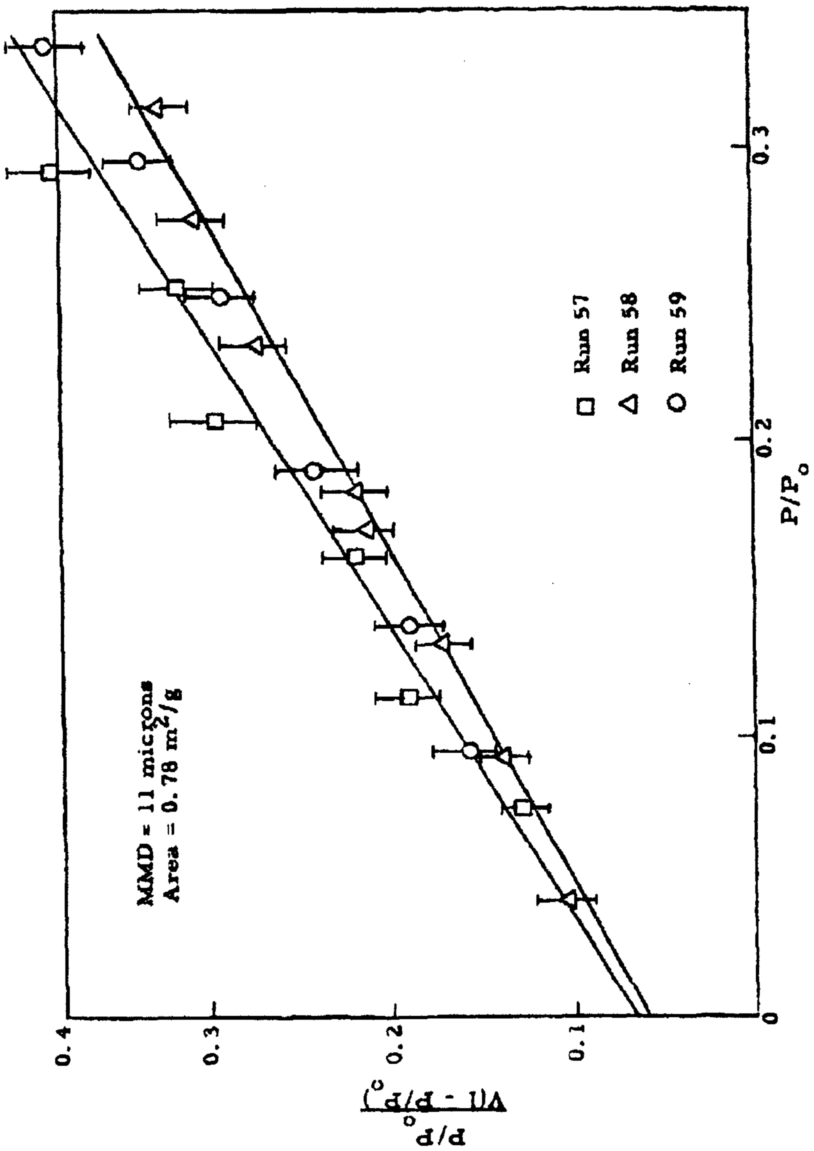

Figure 3.6. BET Plot of N_2 Adsorption Data on Agent LX

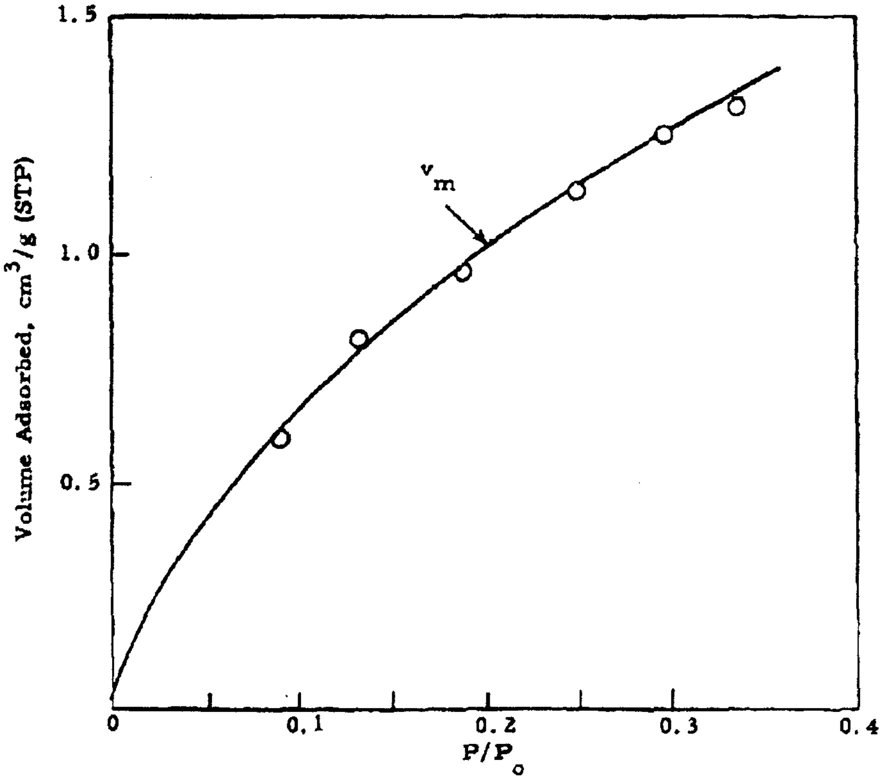

Figure 3.7. Partial Isotherm of N_2 Adsorption on Agent LX at Liquid N_2 Temperature

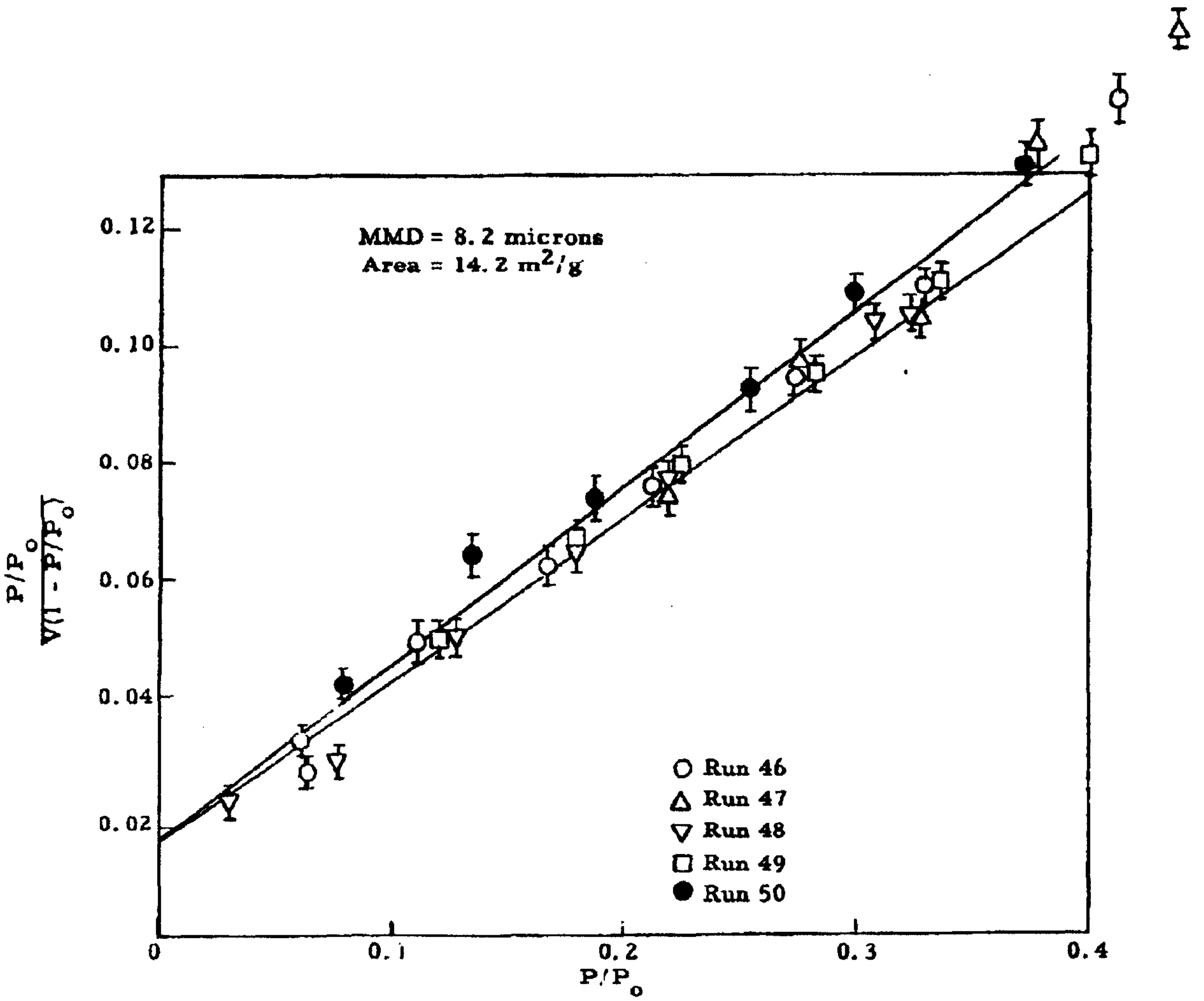

Figure 3.8. BET Plot of N_2 Adsorption on Egg Embryo Showing Normal Error

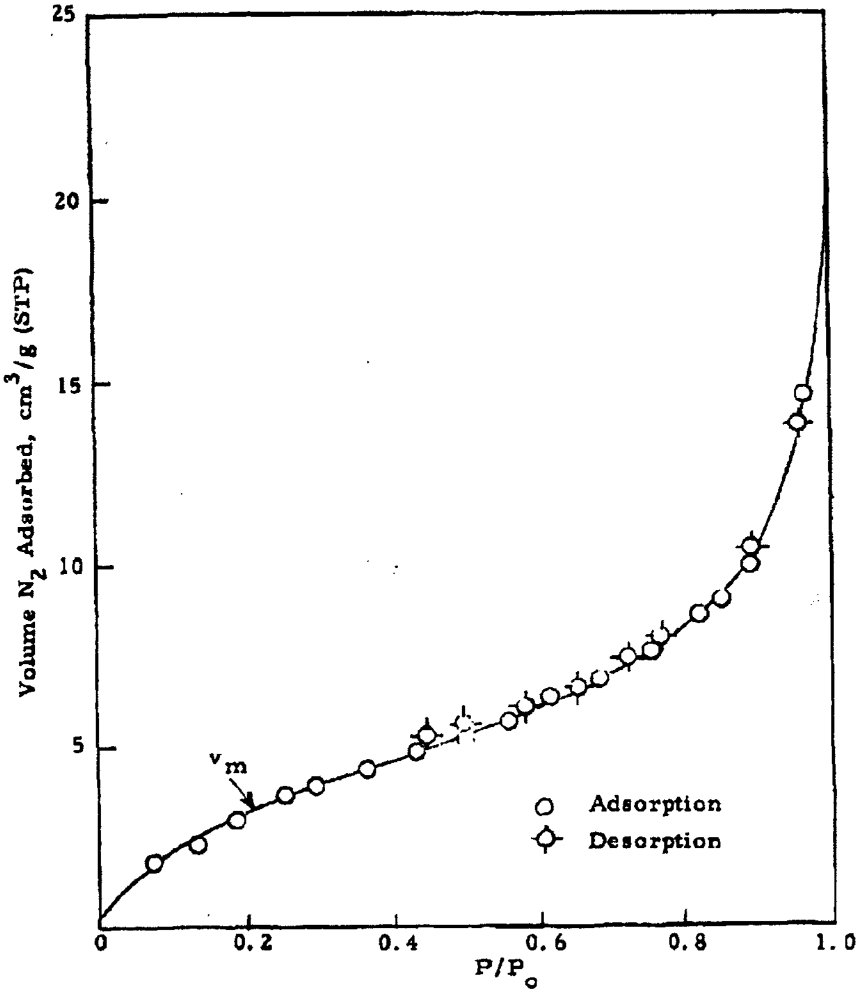

Figure 3.9. Adsorption Isotherm of N_2 on Egg Embryo at Liquid N_2 Temperatures

Egg embryo and agent LX both exhibit the adsorption phenomenon first observed with the other freeze-dried material, Sm[8], i.e., that the surface seems quite inactive. The relative pressure at which the monolayer is completed is approximately 0.2. Also the value of C* in both cases is approximately 20. It is interesting that this characteristic holds for both materials: egg embryo is freeze-dried, but it is not known whether or not agent LX is; this seems to indicate that freeze-drying produces an inactive surface.

3.2. Particle Shape

3.2.1. Shadow-Casting for Electron Micrographs

During the past quarter we have spent a considerable amount of time investigating the techniques necessary for shadow-casting samples that are to be observed in the electron microscope. In the process we found it necessary to modify our vacuum system in order to fulfill the requirements for shadow-casting with chromium. The methods used are similar to those discussed by Hall[10] and by Fischer[11].

In general, shadow-casting will aid in determining the structure of a particle in that the height of the particle can be obtained from the shadow length, and the particle structure in the third dimension is given by the shadow structure. The usefulness of shadow-casting in determining true particle shape is shown by the simple example in Figure 3.10 where a shadowed cross is viewed from the top. It is also found that shadow-casting can be useful in some cases for enhancing the details of the surface structure.

---

*C is related to the average heat of adsorption of the first layer by

$$C = \exp\left[E_{net}/RT\right] \qquad (23)$$

where C = constant of the BET equation
R = gas constant
T = absolute temperature.

(Equation 23 corrects the one appearing in the Thirteenth Quarterly Report, p. 3-14.)

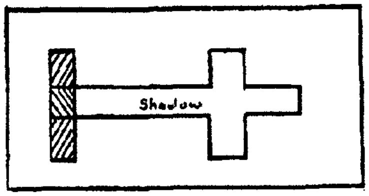

Figure 3.10. Sketch of Shadow-Cast Cross Viewed from the Top

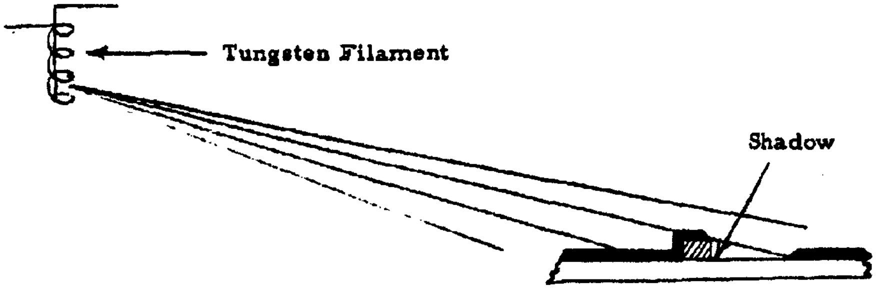

Figure 3.11. Sketch of Shadow-Casting Process

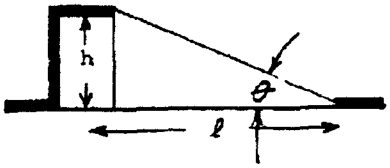

Figure 3.12. Geometry of Shadow

Basically, shadow-casting is the evaporation of a metal from a distant source located at a shallow angle with respect to the surface of the sample substrate. Several metals are suitable for shadow-casting--including gold, chromium, uranium, and germanium. Figure 3.11 gives a diagram illustrating the shadow-casting process (located in a vacuum system). Metal is evaporated from a tungsten filament that is wound in the shape of a wire basket. If the pressure in the vacuum system is low enough (about 10^{-5} mm Hg) the evaporated metal travels in straight lines and is deposited on all surfaces facing the filament. Regions behind a particle will not receive a metal deposit and thus will be detected as a "shadow" in the electron microscope. The height of the particle (Figure 3.12) is given by the relation $h = l \tan \theta$, where l and θ are determined geometrically.

The shadow-casting process requires a vacuum system and a low voltage-high current power supply. The only requirement of the power supply is that it supply sufficient power to the filament in order to reach the evaporation temperature of the metal. The vacuum system must have vacuum pumps that are capable of maintaining a good vacuum throughout the evaporation process. It is imperative that a good vacuum be maintained at all times since, as the pressure inside the vacuum system increases, the metal rays are scattered more strongly by the residual gas molecules. The resulting shadows become diffuse (in an extreme case, the shadows may disappear).

The thickness of the shadow film is determined electrically by measuring the resistance of the film deposited on a glass slide. This enables us to produce films of desired thickness in any given experiment. In general, a thick shadow film is used to determine gross structure while thinner films are used to determine finer detail.

3.2.2. Egg Embryo

The value of shadow-casting in determining the 3-D structure of particles is illustrated by the electron micrographs of egg embryo particles shown

Page determined to be Unclassified
Reviewed Chief, RDD, WHS
IAW EO 13526, Section 3.5
Date: JUL 19 2013

in Figures 3.13, 3.14, and 3.15. Figure 3.13 is of particular interest for it shows how the fine particles of egg embryo can have a very loose structure. One can see how much information shadow-casting adds if one views these photographs while imagining that the shadows are not there.

These photographs also point out a possible problem that may arise in the observation of fine particles with light or electron microscopes: The influence that the dispersing process may have on the apparent particle structure.

In the photographs of egg embryo, two dispersing processes are used. In one method the powder is ultrasonically dispersed in butyl alcohol and then sprayed on the grid with an air gun (similar to a paint sprayer). In the second method, a small amount of powder is placed on a glass slide and then dispersed (dry) by discharging a spark through the powder with a telsa coil (Ref. 11, p. 127). The photographs of egg embryo illustrate our general observations. The dry (spark) dispersed particles are composed of subparticles that are appreciably smaller than the subparticles of the butyl alcohol dispersed particles (which tend to lay flat on the surface). This suggests that the subparticles in these photographs are actually agglomerates of very small particles. If this is the case, the larger subparticles observed with the butyl alcohol dispersing method could be formed during the evaporation of the spray droplets from the grid. This process would also tend to cause the subparticles to lie flat on the grid surface, as is observed. The ultrasonic process could break up the particles of egg embryo allowing them to reform somewhat during the evaporation of the alcohol. We believe that the dry (spark) dispersing method is better for observing fine particles.

It appears as though the fine particles of egg embryo, shown in Figures 3.13, 3.14, and 3.15, are silica. These particles (including the subparticles) are similar in appearance to photographs of Cab-O-Sil (silica formed by a vapor phase process) appearing in Ref. 12. The larger particles shown in Figure 3.16 (also shown in Ref. 8 as Figure 3.13, p. 3-24) are probably

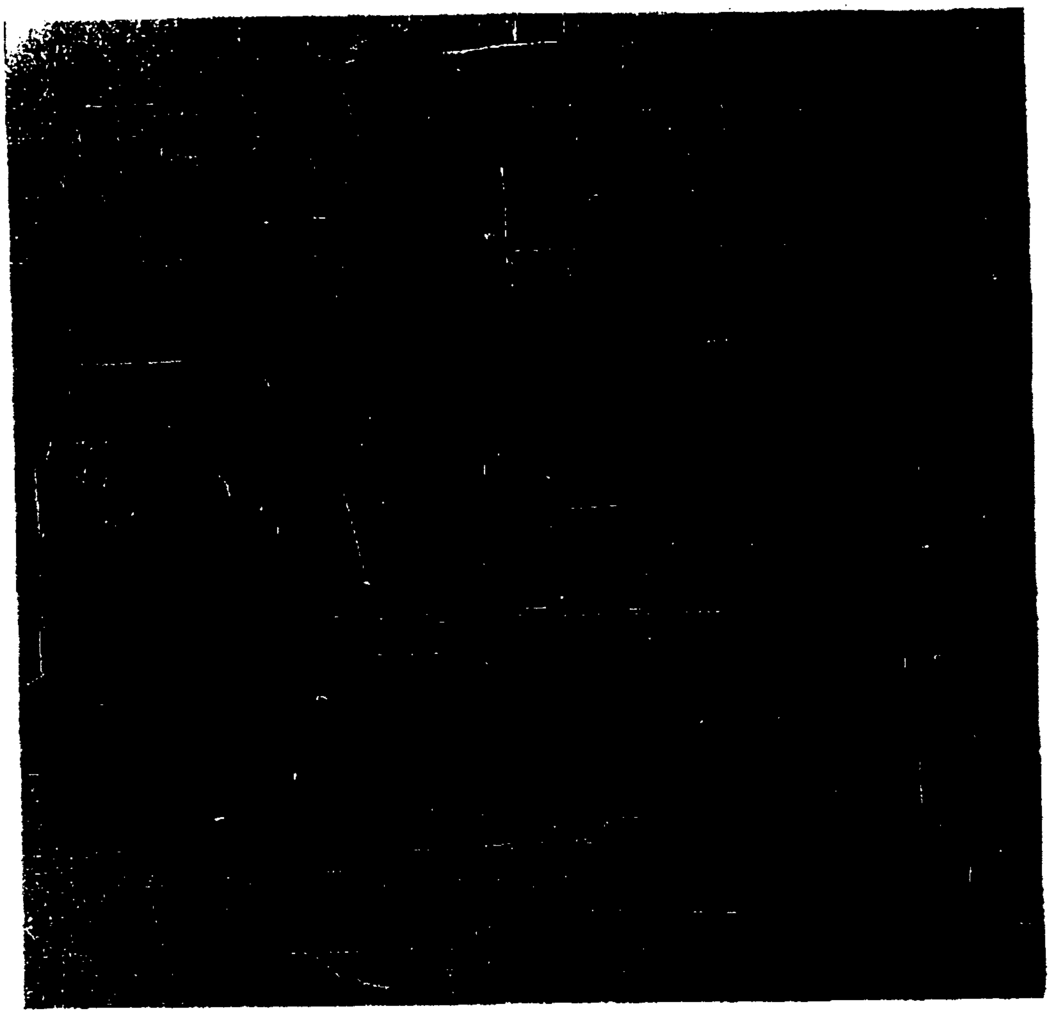

Powder Egg Embryo MMD (Whitby) 8.2 microns

Method of Dispersion Spark Discharge

(shadow-cast with chromium at a 1 to 4 height-to-length ratio)

Magnification 28,000 x (microscope) 2.5 x (enlargement) 70,000 x total

Micrograph No. 63-10-23

Figure 3.13. Electron Micrograph of Shadowed Egg Embryo

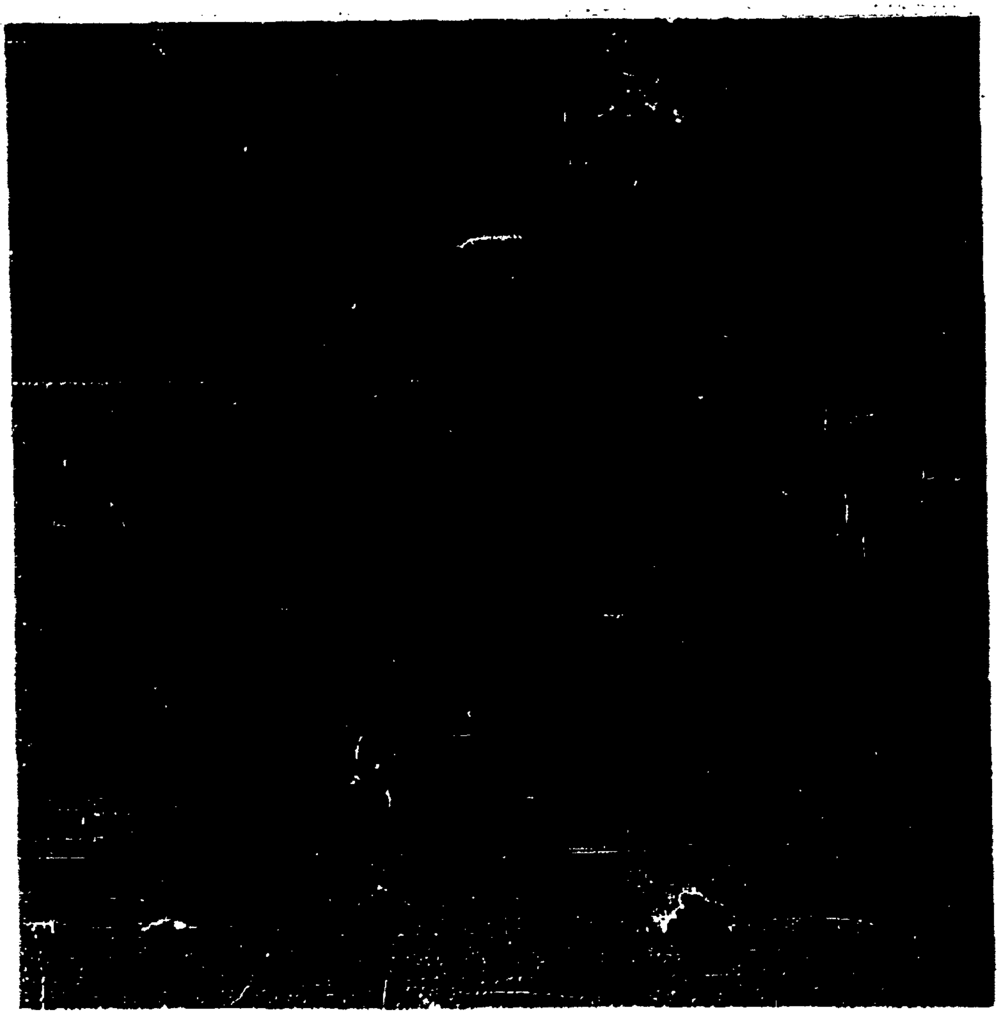

Powder Egg Embryo MMD (Whitby) 8.2 microns

Method of Dispersion Pressed on Grid and Blown off with Air

(shadow-cast with chromium at a 1 to 4 height-to-length ratio)

Magnification 28,000 x (microscope) 2.5 x (enlargement) 70,000 x total

Micrograph No. 63-10-29

Figure 3.14. Electron Micrograph of Shadowed Egg Embryo

Powder Egg Embryo MMD (Whitby) 8.2 microns

Method of Dispersion Ultrasonic Dispersed in Butyl alcohol; sprayed on with air gun

Magnification 28,000 x (microscope) 2.5 x (enlargement) 70,000 x total

Micrograph No. 63-9-36

(shadow-cast with chromium at a 1 to 4 height-to-length ratio)

Figure 3.15. Electron Micrograph of Shadowed Egg Embryo

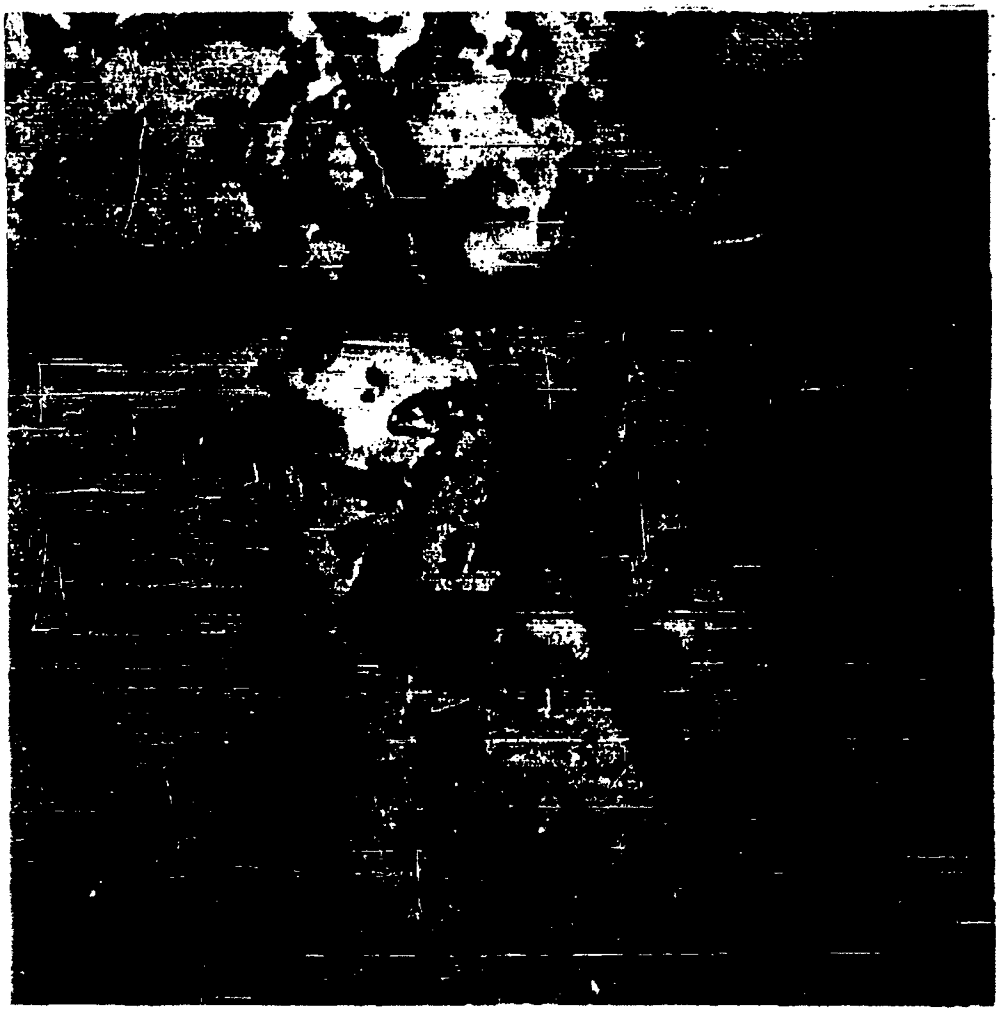

Powder Egg Embryo **MMD (Whitby)** 8.2 microns

Method of Dispersion Spark Discharge

Magnification 100 x (microscope) 2 x (enlargement) 200 x total

Micrograph No. 63-10-5

Figure 3.16. Light Micrograph of Egg Embryo

composed of lactose (transparent particles) surrounding small silica particles. These larger lactose particles may have egg embryo on the surface (this appears as opaque portions).

To test the above hypothesis, egg embryo was dispersed on a glass slide and then photographed with the use of a light microscope. The slide was then carefully placed in distilled water for 40 hours, removed, and again photographed (the same area being photographed each time). The two photographs are shown in Figures 3.15 and 3.17. We see that all the transparent portions of the particles are dissolved in the water; this supports our supposition that these are composed largely of lactose. In the place of these transparent portions, are left small particles (presumably silica) and larger opaque regions (possibly egg embryo). We see that the remaining small particles shown in Figure 3.17 form patterns which closely correspond to the original particles (Figure 3.15). This indicates that the transparent particles are dissolved but not washed away. Another experiment determined that approximately 45 percent of the egg embryo powder is water soluble. .

3.2.3. Spray-Dried Saccharin

Some work has also been done on spray-dried saccharin. Photographs of this powder are shown in Figures 3.18 and 3.19. This powder appears to have a very smooth surface and is very spherical. The good spherical shape is of special interest since the properties of spheres are generally much easier to analyse than the properties of powders with irregular shapes.

3.2.4. Agent LX

Figures 3.20 through 3.25 show the structure of agent LX. Figure 3.20 shows the general powder structure as observed in the light microscope. Figures 3.21, 3.22, and 3.23 show some of the smaller particles observed in the electron microscope.

Powder Egg Embryo MMD (Whitby) 8.2 microns

Method of Dispersion Spark Discharge

(Figure 3.16 powder dissolved in H_2O and dried)

Magnification 100 x (microscope) 2 x (enlargement) 200 x total

Micrograph No. 63-10-5[1]

Figure 3.17. Light Micrograph of Egg Embryo

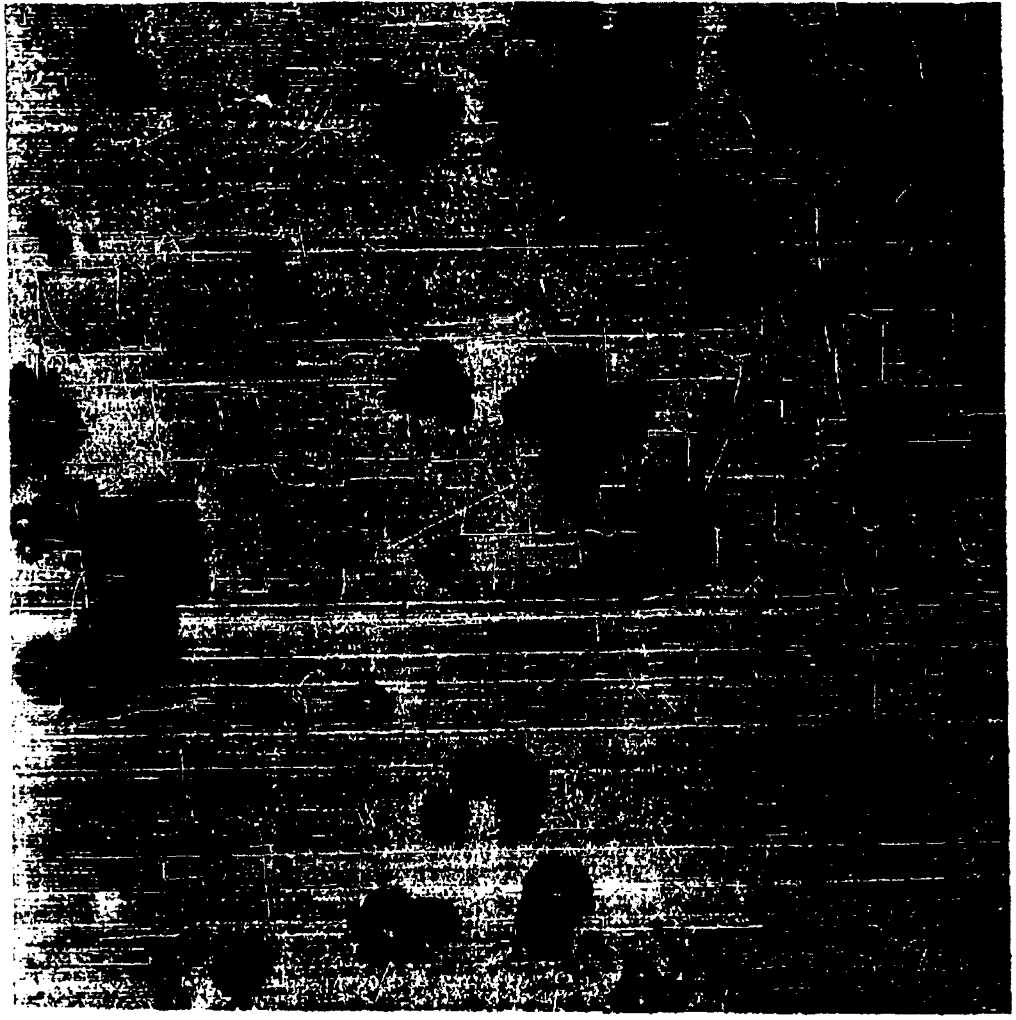

Powder Spray-Dried Saccharin **MMD (Whitby)** 12 microns

Method of Dispersion Spark Discharge

Magnification 400 x (microscope) 2 x (enlargement) 800 x total

Micrograph No. 63-11-10

Figure 3. 18. Light Micrograph of Spray-Dried Saccharin

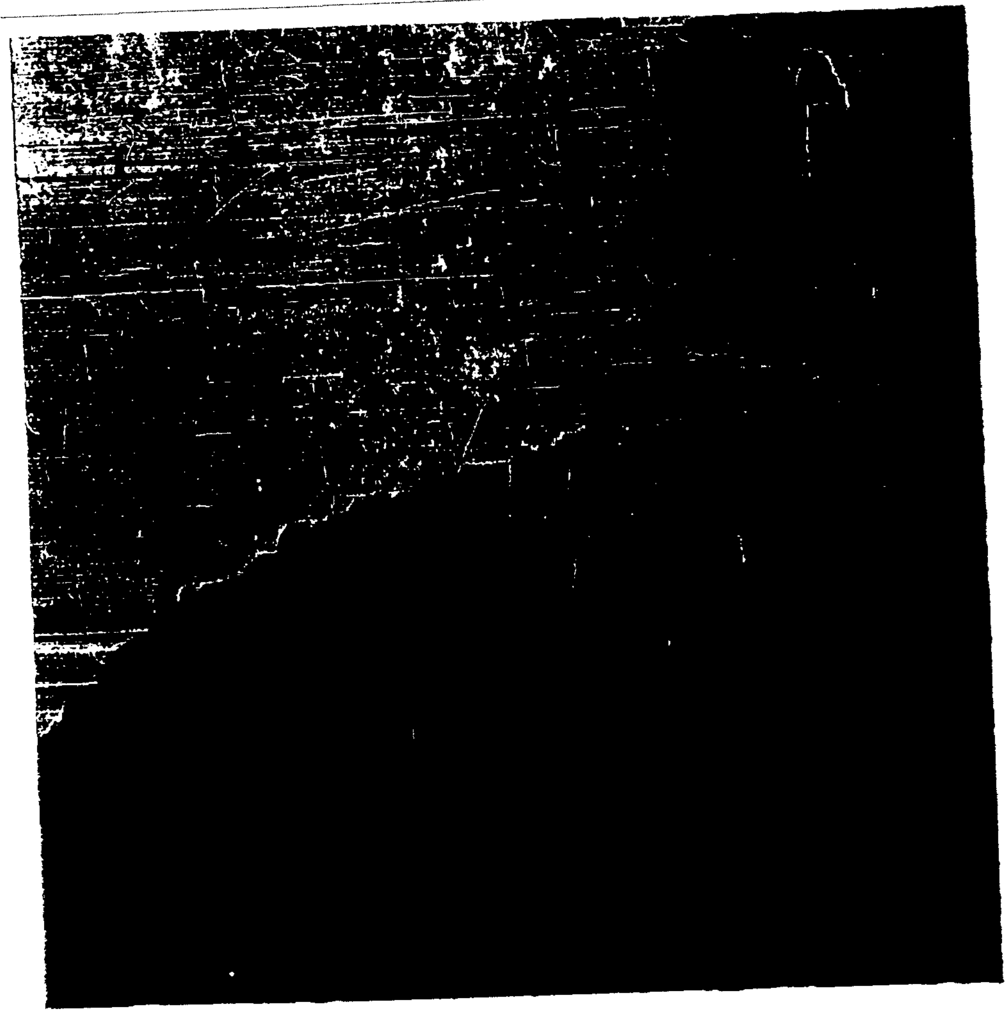

Powder Spray-Dried Saccharin **MMD (Whitby)** 12 microns

Method of Dispersion Spark Discharge

Magnification 11,000 (microscope) 2.5 x (enlargement) 27,500 x total

Micrograph No. 63-11-6

Figure 3.19. Electron Micrograph of Spray-Dried Saccharin

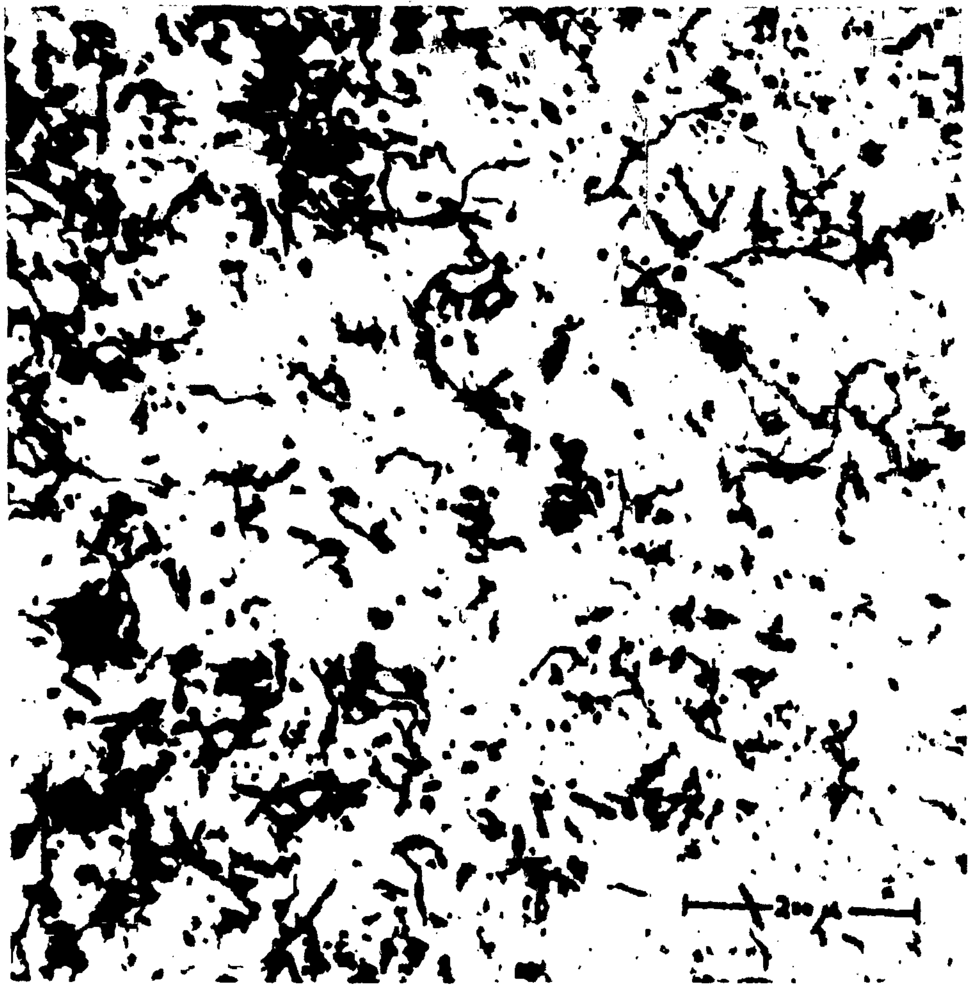

Powder Agent LX **MMD (Whitby)** 8 microns

Method of Dispersion Spark Discharge

Magnification 100 x (microscope) 2 x (enlargement) 200 x total

Micrograph No. 63-11-15

Figure 3.20. Light Micrograph of Agent LX

Powder Agent LX **MMD (Whitby)** 8 microns

Method of Dispersion Spark Discharge

Magnification 4700 x (microscope) 2.5 x (enlargement) 11,700 x total

Micrograph No. 63-11-11

Figure 3.21. Electron Micrograph of Agent LX

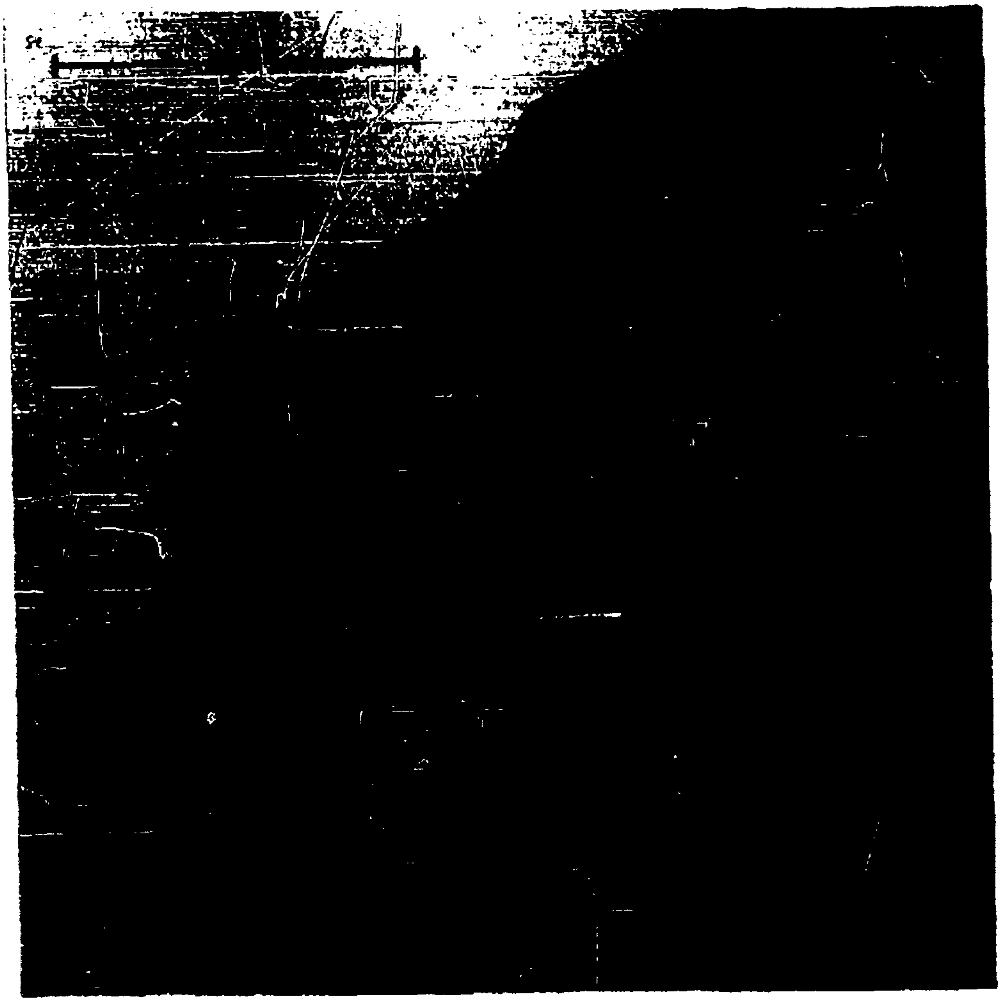

Powder Agent LX **MMD (Whitby)** 8 microns

Method of Dispersion Spark Discharge

Magnification 4700 x (microscope) 2.5 x (enlargement) 11,700 x total

Micrograph No. 63-11-20

Figure 3.22. Electron Micrograph of Agent LX

Page determined to be Unclassified
Reviewed Chief, RDD, WHS
IAW EO 13526, Section 3.5
Date: JUL 19 2013

Powder Agent LX **MMD (Whitby)** 8 microns

Method of Dispersion Spark Discharge

Magnification 9,700 x (microscope) 2.5 x (enlargement) 24,200 x total

Micrograph No. 63-11-21

Figure 3.23. Electron Micrograph of Agent LX

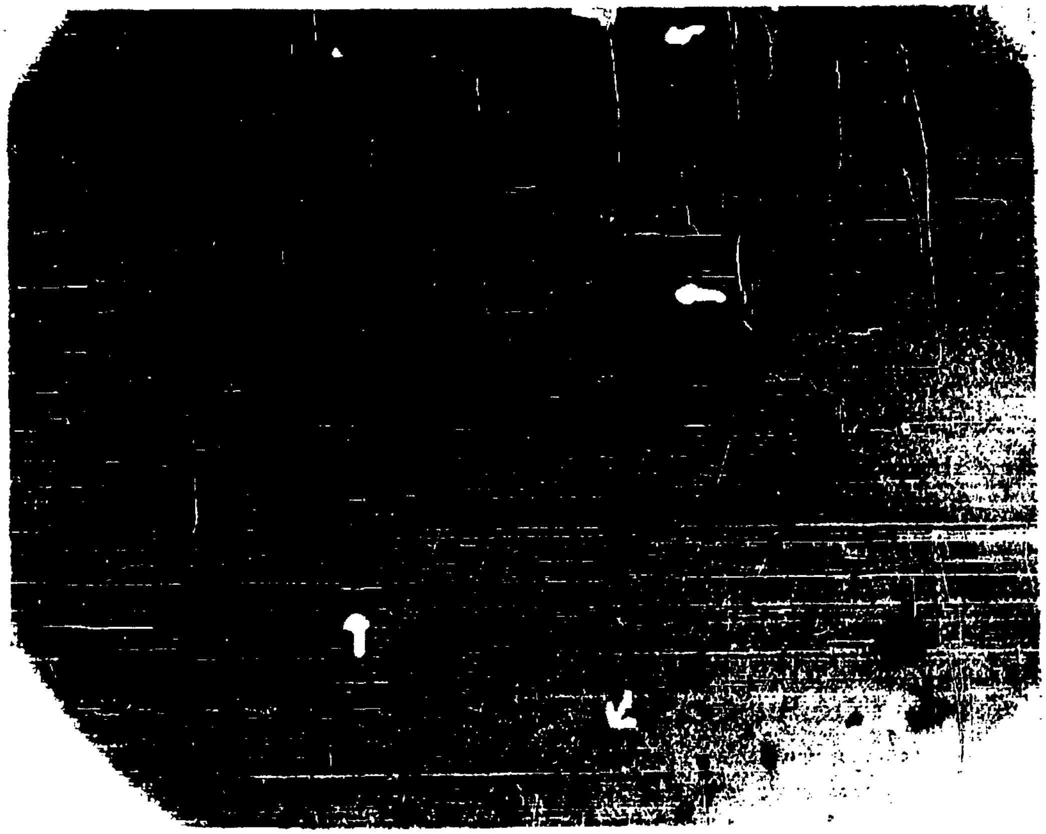

Powder Agent LX **MMD (Whitby)** 8 microns

Method of Dispersion Spark Discharge

Magnification 100 x (microscope) 2 x (enlargement) 200 x total

Micrograph No. 64-1-2

Figure 3.24. Light Micrograph of Agent LX

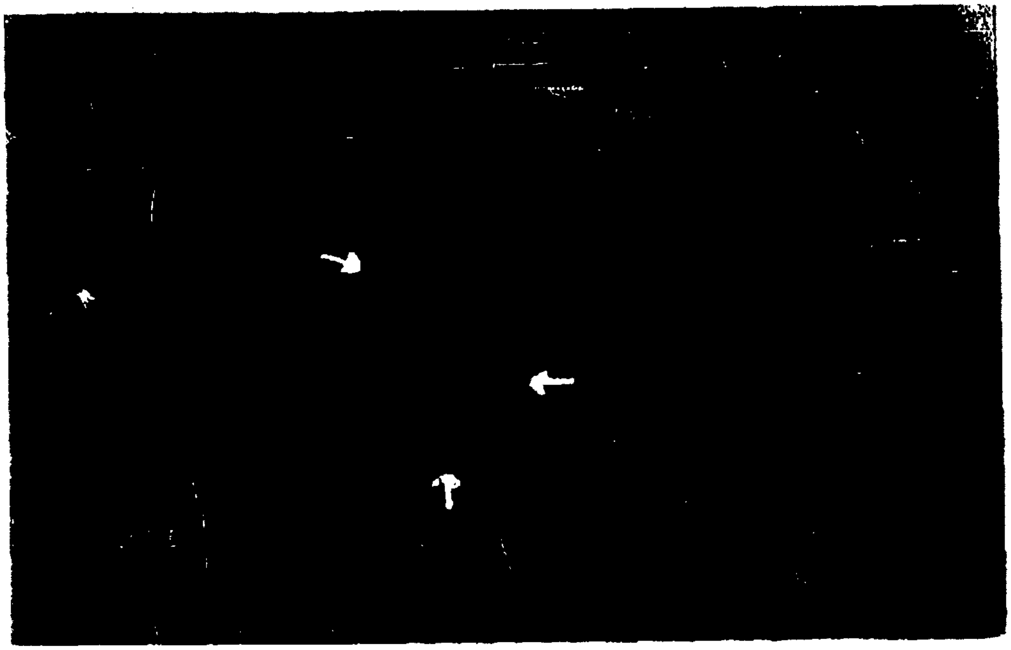

Powder Agent LX **MMD (Whitby)** 8 microns

Method of Dispersion Spark Discharge

(submerged in distilled water)

Magnification 100 x (microscope) 2 x (enlargement) 200 x total

Micrograph No. 64-1-1

Figure 3.25. Light Micrograph of Agent LX

These photographs show that agent LX is another powder with highly irregular shape. This irregularity is mainly due to the large amount of debris contained in the powder. The cells are not easily recognized in the dry state. When the powder is submerged in water, however, these cells are immediately observable because they change to a uniform size and shape that are quite different from the debris. Upon drying, the cells again blend in with the background debris; but knowing of their existence and appearance, they can be readily observed. The difference in the cell size and shape under wet and dry conditions is shown in Figures 3.24 and 3.25. This change takes place rapidly upon immersion in water or drying (within 2 or 3 seconds).

3.3. Particle Size Distribution and Particle Density

Particle size distributions of Bg lot 17, Bg lot SCH-63-109, and agent LX, as determined by the Whitby technique, are presented in Figure 3.26.

We employed our usual schedule for size analysis of the Bg samples. For agent LX, compatible liquids and the true particle density were determined before a schedule could be calculated. Benzene was used as the settling liquid and an 85 to 15 volume ratio of benzene to naptha was the dispersing liquid. Solubility of the agent LX in these liquids was negligible as determined by an analysis of the radiation transmission at various wave lengths. A true particle density of 1.34 g/cm^3 was determined by a liquid displacement technique using a vacuum-insulated volumetric flask.

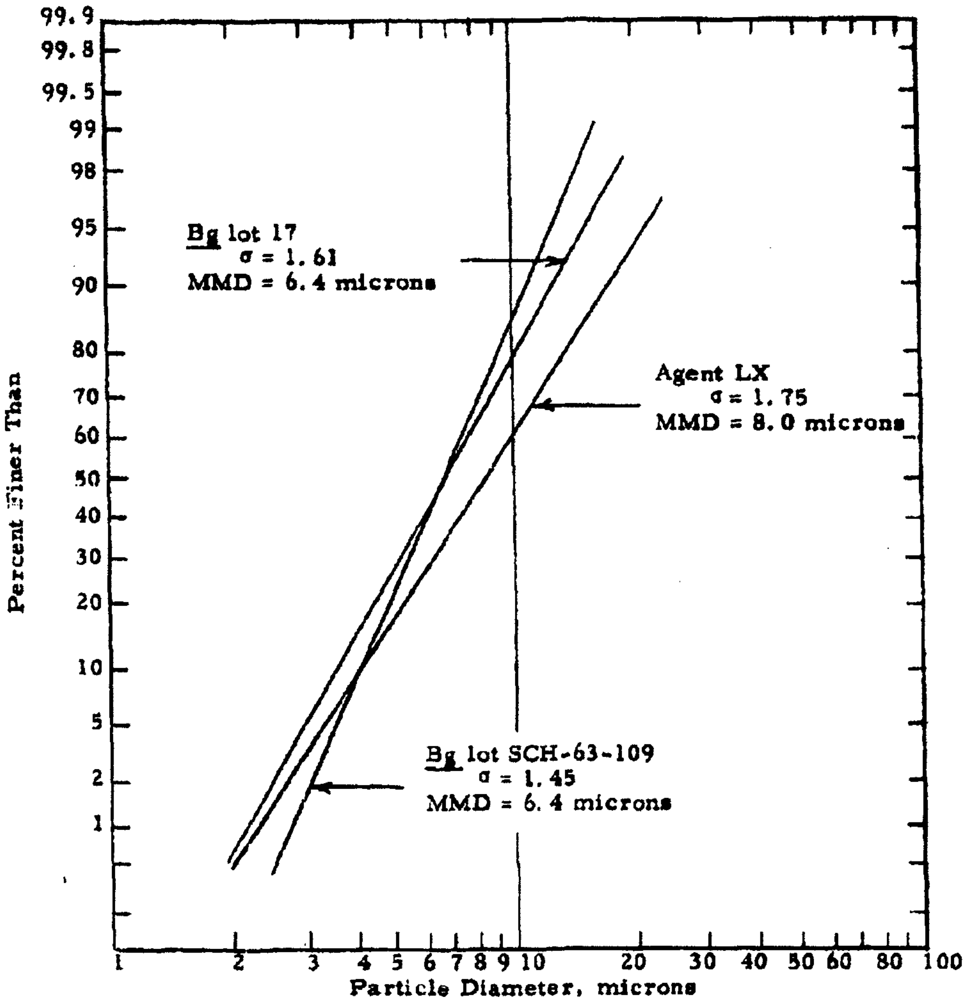

Figure 3.26. Particle Size Distribution of Bg and Agent LX

4. AEROSOL STUDIES

The previous work on the effects of receptacle atmosphere humidity upon formation and decay of aerosols has been limited to three cases: low humidity (5 percent or less), room humidity, and high humidity (95 percent or greater). During the fourteenth quarter provisions were made for the initial aerosol chamber humidity to be set to any prescribed level. A series of runs, using powdered sugar, was then conducted at initial chamber humidities covering the full range of 0 to 100 percent. The results of these runs are discussed in the present report.

4.1. Operating Procedure

The operating procedure was discussed rather fully in the Thirteenth Quarterly Report. In the present quarter the powder sample handling, standardization of the optical system, and data reduction were exactly as described in sections 4.1.1, 4.1.3, and 4.1.5, respectively, of that report. Furthermore, the powder-dispersing procedure was the same as that described in the paragraph on "humidity runs" in section 4.1.4. The aerosol chamber humidity control and measurement, however, were different.

Chamber humidity was controlled in the present work by connecting a flushing arrangement to the chamber. In this system, air was either bubbled through a water flask or passed through a desiccant bed before being used to flush the aerosol chamber. The changing chamber humidity was then continuously monitored by one of two methods; when the desired humidity was reached, the conditioning system was shut down and the run initiated.

Chamber humidities lower than 70 percent were measured by an infrared hygrometer which sampled air from the chamber through a long copper tube. This method was not applicable to higher humidities, probably because of water condensation at cold spots in the sampling tube. For the higher humidities, measurements were made by means of a psychrometer installed in the chamber near the fan. The psychrometric method is better suited to the measurement of high humidities since errors, if any, will be in the direction of too high readings.

4.2. Experimental Work and Results

A series of runs at various chamber humidities was conducted for powdered sugar aerosols. The size analysis of the powdered sugar gives

$$\text{MMD} = 5.8 \text{ microns}$$

$$\sigma_g = 1.74.$$

The number median diameter (NMD = d_g) of the sample may be computed from

$$\frac{\text{MMD}}{\text{NMD}} = e^{3 \ln^2 \sigma_g}; \qquad (24)$$

we obtain

$$\text{NMD} = 2.3 \text{ microns}.$$

Figures 4.1, 4.2, and 4.3 show the aerosol "half-life", initial amplitude, and "slope index", respectively, of the various runs plotted against relative humidity of the chamber at the inception of the run.

It is seen in Figure 4.1 that the aerosol half-life increases uniformly with humidity from 5 min at low humidity to 7 min at the high end. The increase is thus 40 percent over the range. The scatter of the data is quite small for this type of experiment. Thus, half-life is an aerosol parameter that can be determined experimentally with acceptable precision. We shall attempt to delve into the significance of this parameter in section 4.2.

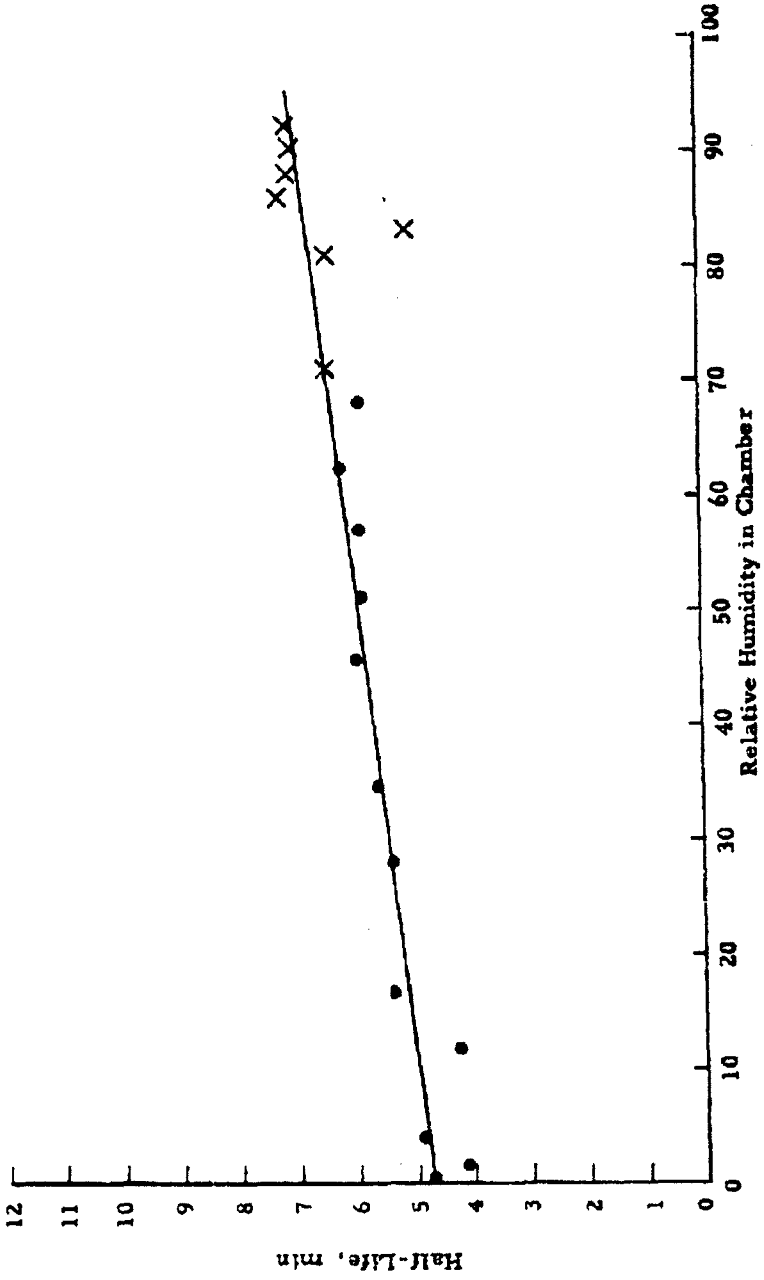

Figure 4.1. Aerosol Half-Life vs. Chamber Humidity

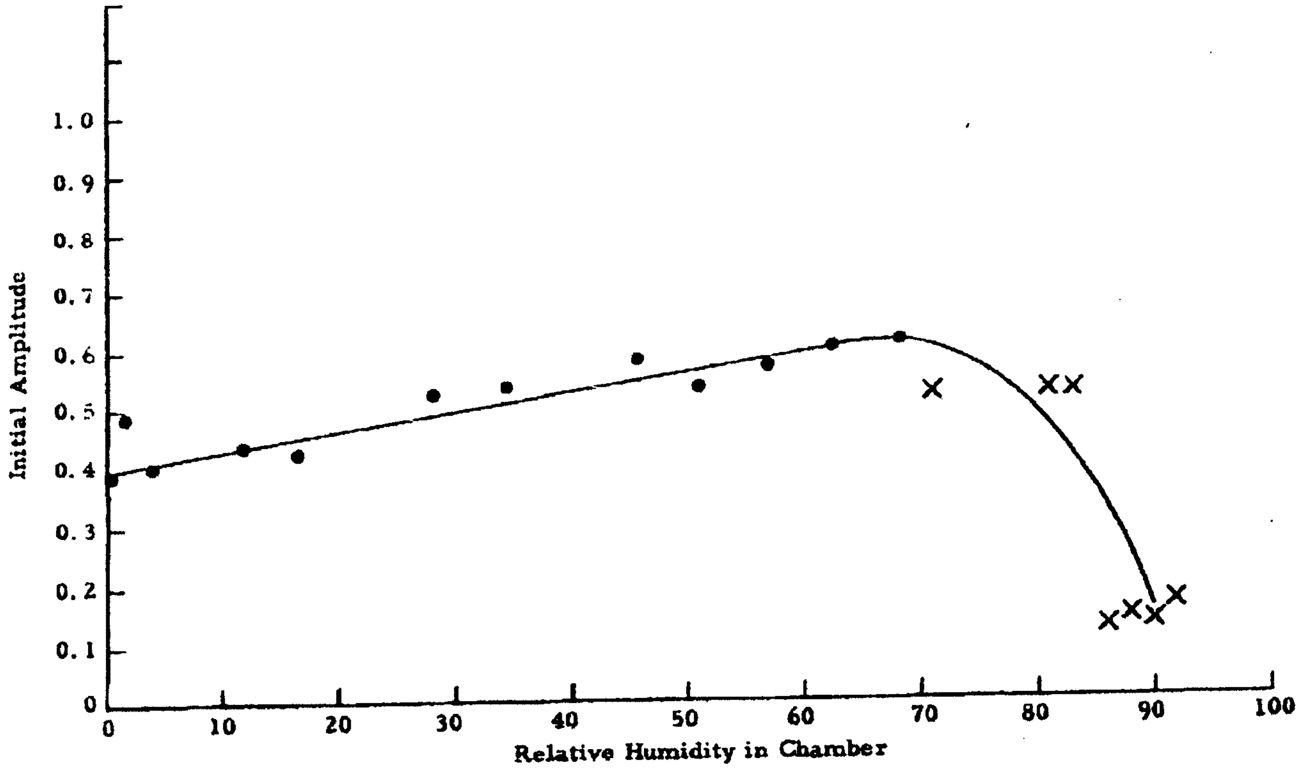

Figure 4.2. Initial Signal Amplitude vs. Chamber Humidity

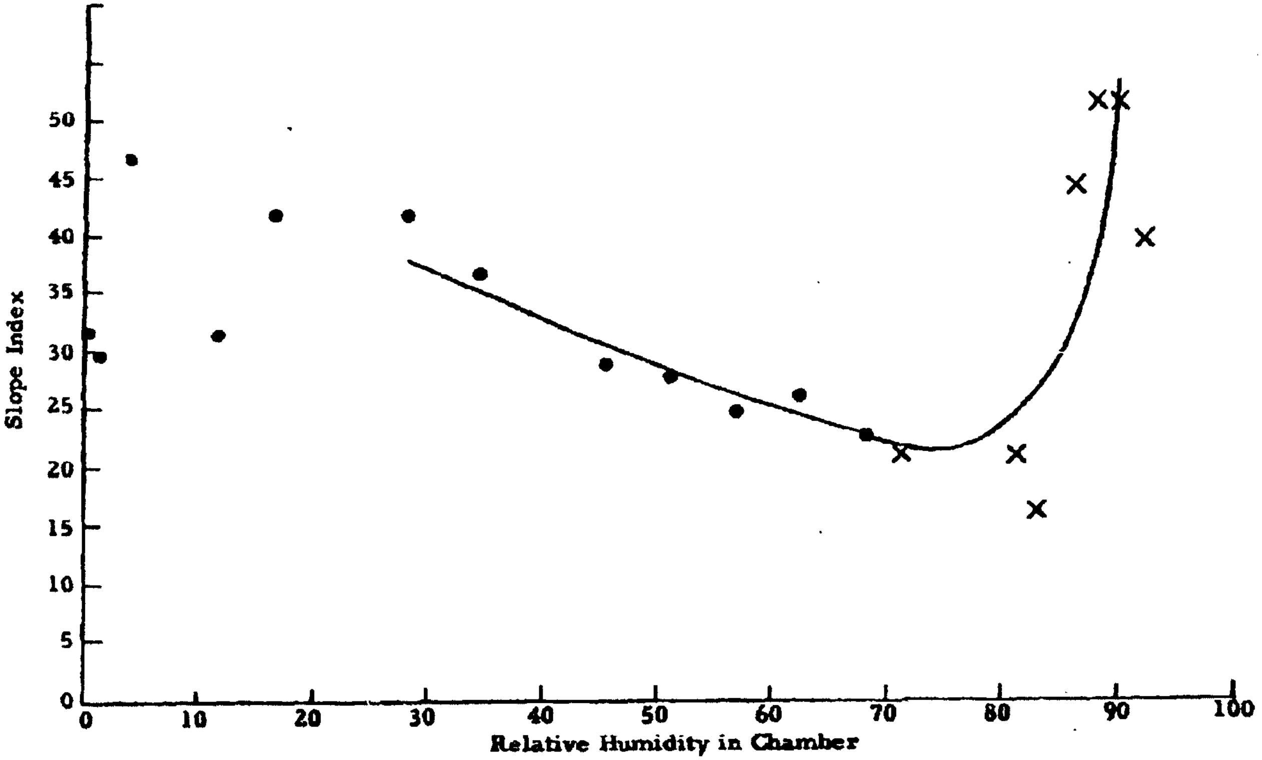

Figure 4. 3. Slope Index for Aerosol Runs vs. Chamber Humidity

The aerosol initial amplitude is shown in Figure 4.2. This parameter, too, exhibits acceptably small scatter. It increases gradually and uniformly from low humidity to about 70 percent, then drops rather sharply at 85 percent. The curve could have been drawn to indicate a precipitous drop from 0.45 to 0.15 at 85 percent. The fact that it is drawn to indicate a smooth roll-off reflects the belief that powder properties (and, therefore, aerosol parameters) change gradually--not discontinuously--with humidity.

Figures 4.1 and 4.2 may be compared with Figures 4.1 and 4.2 of the Thirteenth Quarterly Report. (For comparison purposes, we may take 12 g H_2O/m^3 = 50 percent relative humidity.) Half-lives compare quite favorably, but there is a significant difference in the initial amplitude. The data on initial amplitude secured during the thirteenth quarter reveal values about 2-1/2 times those secured during the fourteenth quarter. This difference is possibly attributed to the fact that the sugar used in the previous period was ground in the winter (10 percent laboratory R. H.), whereas the sugar used during the current quarter was ground during the summer (50 percent R. H.) resulting in the possible formation of a few hard agglomerates. This would result in lowering the initial amplitude. To overcome this problem, a facility is being constructed to permit grinding of the powders in a completely controlled atmosphere.

The aerosol parameter "slope index" is shown in Figure 4.3. This parameter seemed to be well behaved in the range of 30 to 80 percent, decreasing over that range. A sharp upward swing is indicated at about 85 percent.

4.3. Data Analysis

In this section we shall attempt to look more deeply into the significance of the various aerosol parameters. The analysis is based on the theoretical model for the optical properties of a turbulent-decaying, nonagglomerating aerosol first discussed in section 3.2 of the Eighth Quarterly Report.[13] Some aspects of the model were further discussed in the Ninth Quarterly Report (section 3.3) and the whole topic was summarized in more concise form in Appendix A of the Eleventh Quarterly Report.

The model for the optical properties of an aerosol assumes that at some initial time the aerosol particles are uniformly (within the limitations of statistics) distributed throughout the chamber and that the size distribution of the airborne particles can be adequately represented by a log-normal distribution. Presumably this distribution is closely related to the actual size distribution of the powder.

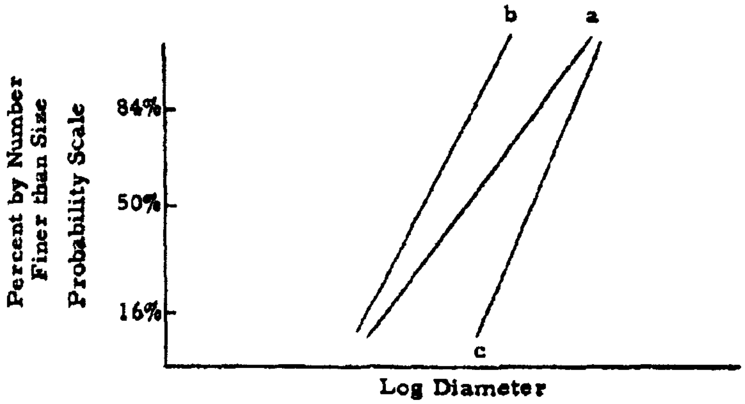

Supposing, in the diagram, that the line "a" is the actual size distribution of the powder sample, then loss of large particles to chamber walls during the dispersing phase would yield the line "b" as the initial airborne size distribution. If incomplete separation or rapid reagglomeration precludes the appearance of fine particles in the initial aerosol, line "c" would result. Other combinations are possible.

The model for nonagglomerative turbulent settling further assumes that the concentration of aerosol particles of size class "d" decreased exponentially with time:

$$e = \frac{-v(d)}{h} t \qquad (25)$$

where $v(d)$ = terminal settling velocity of a particle of diameter d

H = chamber height.

The signal due to the scattering of light by a single particle in the scattering zone is

$S\,(\text{single}_{\text{particle}}) = I\delta\Omega\,\sigma(d)$

I = light beam intensity in photometer units/cm^2

$\delta\Omega$ = geometric factor

$\sigma(d)$ = cross section of particle of diameter d for 90° scattering.

Results quoted in Appendix A of the Eleventh Quarterly Report show that (d) may be approximated by

$$\sigma(d) = \frac{d^m}{K};\ m,\ K = \text{constants.} \qquad (26)$$

In the analysis to follow, we took

$M = 1.6$

$K = 20$

(σ is in square microns if d is in microns).

When these assumptions are combined and the necessary integration performed, it is found that the initial signal amplitude S_o is related to the initial aerosol parameters d_g and σ_g by

$$S_o = I\delta\Omega C\delta V \cdot \frac{d_g^{\;m}}{K}\, e^{\frac{m^2}{2}\ln^2\sigma_g} \tag{27}$$

where C is concentration of the initial aerosol in particles/cc and S_o is the volume of the scattering zone. The time dependence of the signal S is predicted to be log-normal:

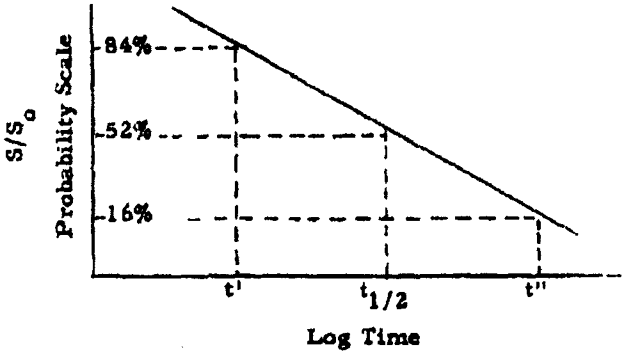

The slope index (= t"/t') is a function of σ_g alone, as shown in Figure A-3 of the Eleventh Quarterly Report. The half-life $t_{1/2}$ is related to the initial aerosol parameters by

$$t_{1/2} \cdot \frac{v(d_g)}{H} \cdot e^{2m\ln^2\sigma_g} \cong 0.65\,. \tag{28}$$

One of the limitations of the aerosol settling expression is that it does not take into account the unknown loss of aerosol particles by impingement on vertical walls. Correction for this would not disturb the relation for the slope index but could change the half-life relation by as much as 40 percent. The d_g calculations by that relation are therefore apt to be too high by 20 percent.

The first step in the reduction of data was to determine the geometric standard deviation σ_g of the initial aerosols. These were found from the measured slope indices by means of the graphic relation between the two quantities. The results, plotted again vs. chamber humidity, are shown in Figure 4.4. The scatter in this plot, which of course reflects the scatter in the measured slope indices, is unfortunate because of the key role played by σ_g in later calculations. We continue, however, and base our judgment on the credibility of later graphs. For comparison, in Figure 4.4, it will be recalled that the GSD of the sugar sample itself was 1.74.

Once the σ_g's are known we may proceed to the initial aerosol d_g. From the relation

$$v(dg) = \frac{0.65\ H}{t_{1/2}\, e^{2m \ln^2 \sigma_g}} . \tag{29}$$

The half-lives and σ_g's determine the settling velocity. Stoke's relation then specifies the d_g's. These are shown in Figure 4.5. We note first that the d_g's are somewhat above the count median diameter of the powder. This is no doubt due in part to the inflation of d_g values by virtue of impingement on walls, but this factor should be constant across the humidity range.

The change of diameter with humidity ought, therefore, be real--although the scale may be too high.

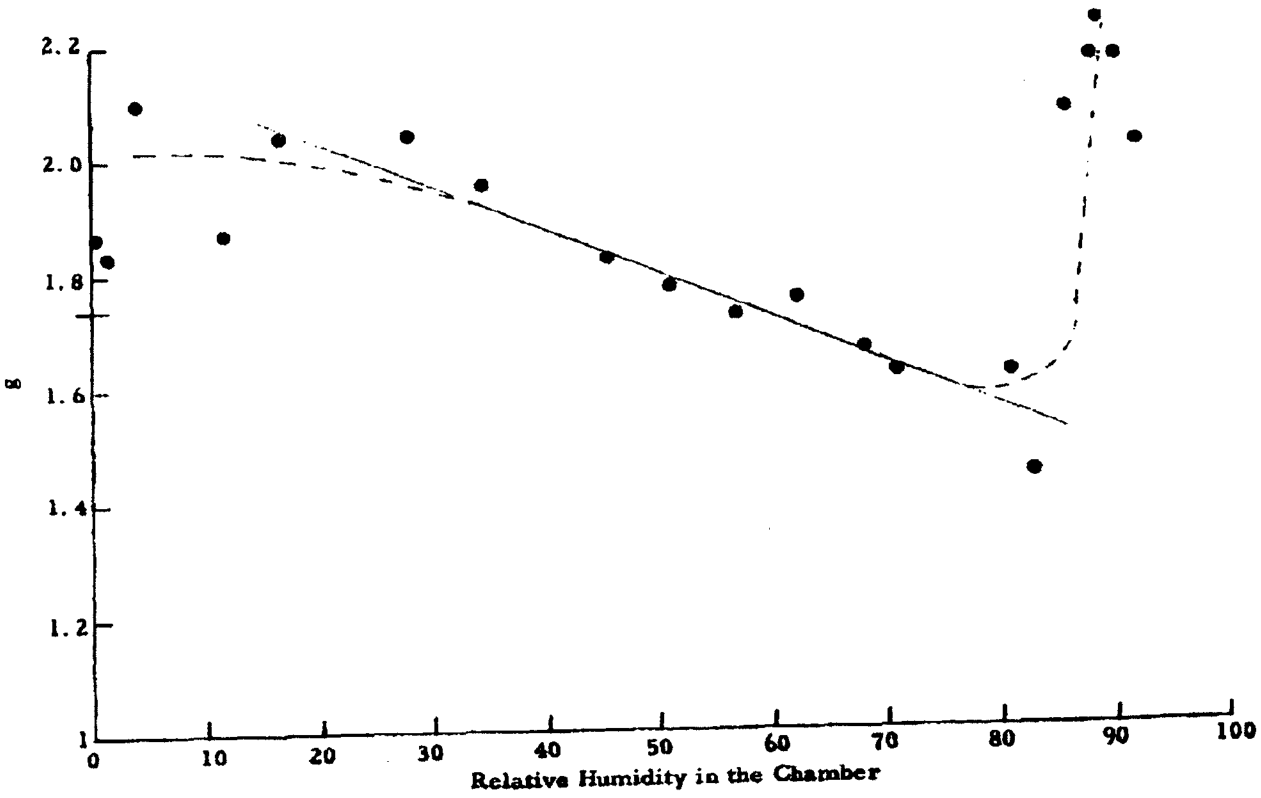

Figure 4.4. Calculated Geometric Standard Deviation of Initial Aerosol vs. Chamber Humidity

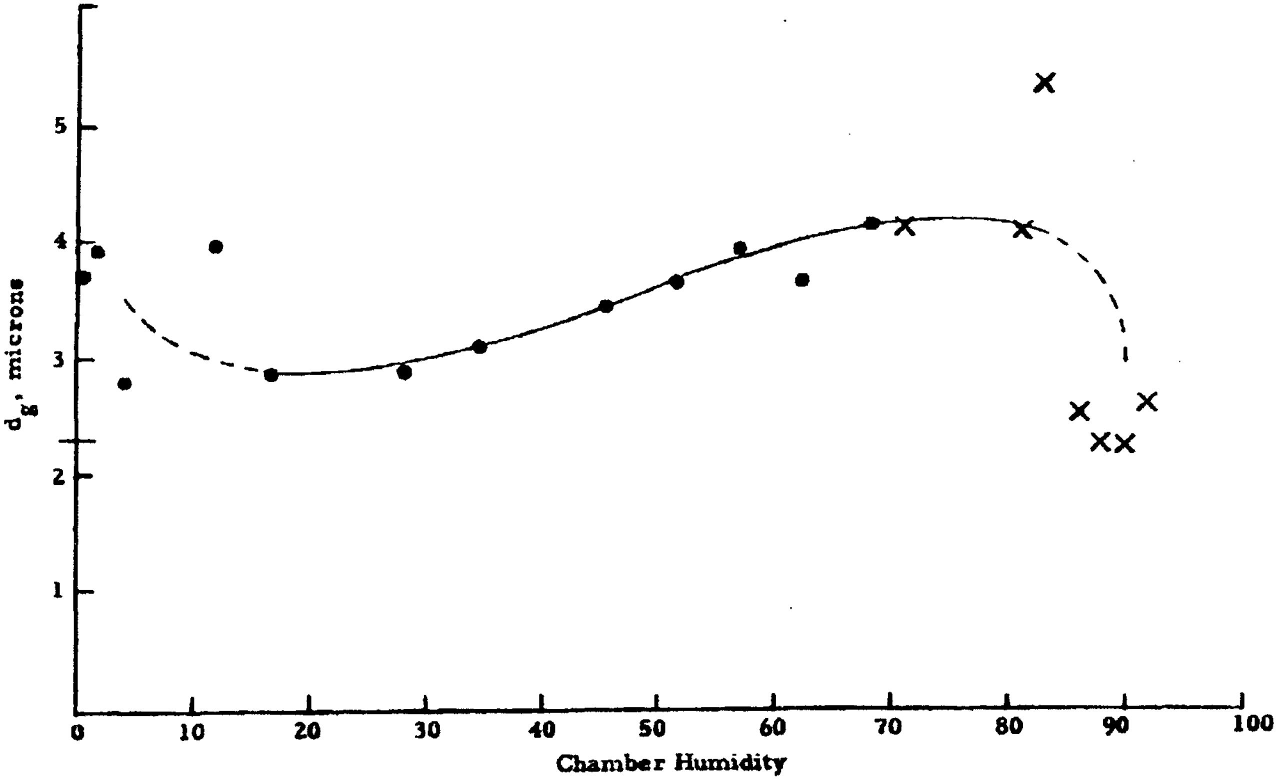

Figure 4.5. Calculated Geometric Mean Diameter of Initial Aerosol vs. Chamber Humidity

Figure 4.5 is surprising. On the basis of Figure 4.1 alone, one is tempted to make the statement that the "typical particle size" (not clearly defined) decreases with increasing humidity; Figure 4.5 indicates a more complicated behavior. In fact, Figure 4.5 shows that d_g (which is a less ambiguous measure of size) increases with increasing humidity over much of the range, then drops sharply at 85 percent.

The intensity of the vertical light beam has been measured (section 3.1.2, Tenth Quarterly Report)[14] and found to be

$$I = 2.1 \times 10^6 \text{ photometer units/cm}^2$$

and the solid angle subtended by the detector is

$$\delta\Omega = 5.38 \times 10^{-3}.$$

The volume of the scattering zone is

$$\delta V = 7.6 \text{ cm}^3.$$

These data, together with d_g, σ_g and the initial signal amplitude, determine the initial aerosol concentration C. C is plotted in Figure 4.6. This quantity is rather constant at 1000 particles/cm^3 over the humidity range of 30 to 70 percent but falls off at either end of that range. Figure 4.6 bears a close resemblance to the initial signal amplitude (Figure 4.2). This justifies the loose identification between the two quantites as made in the past.

A final calculation determines the mass M of powder airborne in the initial aerosol. M is given by

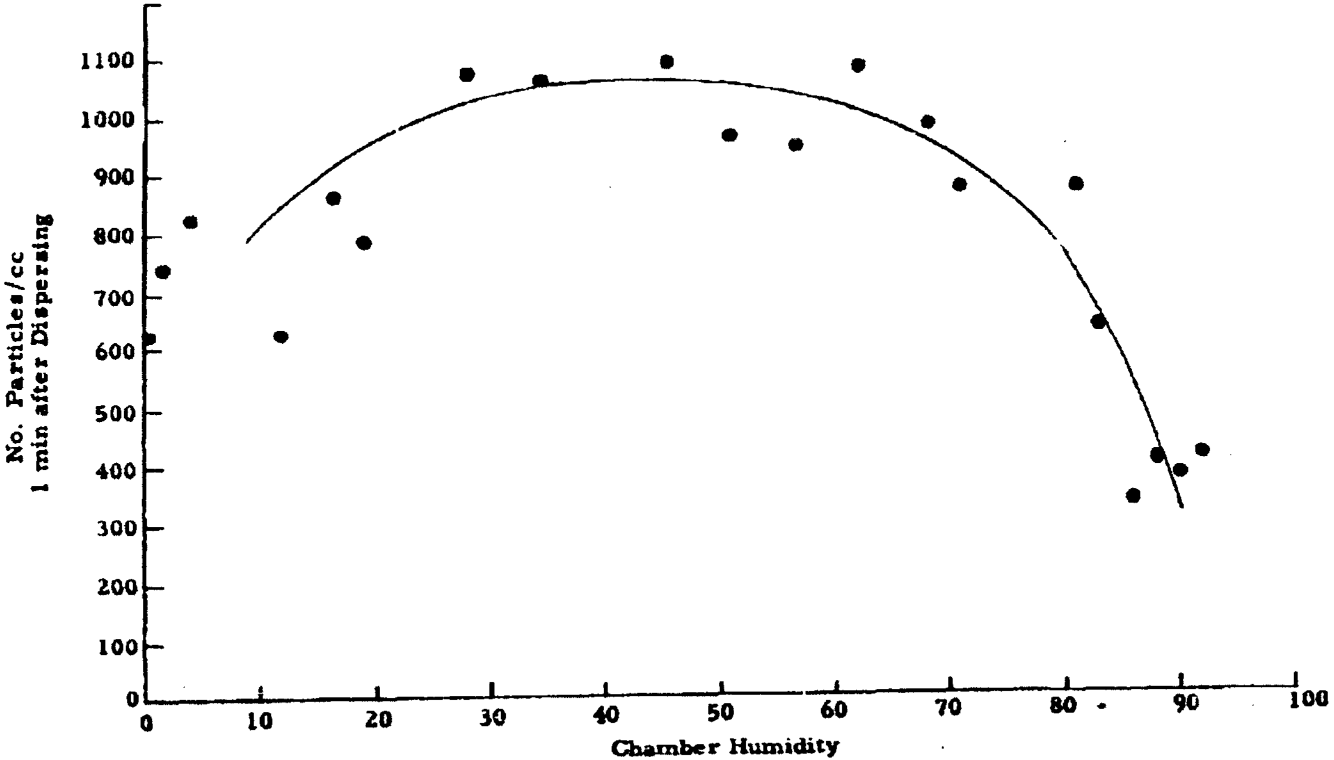

Figure 4. 6. Calculated Initial Aerosol Concentration vs. Chamber Humidity

$$M = C\rho V \frac{\pi}{6} dg^3 e^{9/2 \ln^2 \sigma_g} \qquad (30)$$

where $V = 10^6$ cm^3 is the chamber volume and $\rho = 1.59$ g/cm^3 is the particle density. M is plotted in Figure 4.7. Over much of the humidity range (up to 70 percent) the calculated mass is in the neighborhood of 180 mg. This is impossible since only 100 mg of powder were dispersed in each run. The fact that M is too large by at least a factor of 1.9 probably means that the calculated dg's are too large by a factor of

$$(1.9)^{\frac{1}{3 - m}} = (1.9)^{\frac{1}{1.4}} = (1.9)^{0.712} = 1.58 .$$

It is interesting to note in Figure 4.7 that the scatter of points is no worse (better at low humidities) than in Figures 4.4, 4.5, and 4.6. This is remarkable in that M is proportional to d cubed and to an exponential function of σ_g. The scatter in σ_g, d_g, and C is made more acceptable by the fact that M is left more or less undisturbed.

The curve which best fits the data in Figure 4.7 is perhaps the solid curve shown. This curve indicates that above 60 percent relative humidity, there is increasing difficulty in getting the full powder sample dispersed and airborne. It might be noted, however, that--except for the last four points--the curve might be drawn on the level as shown by the dashed line.

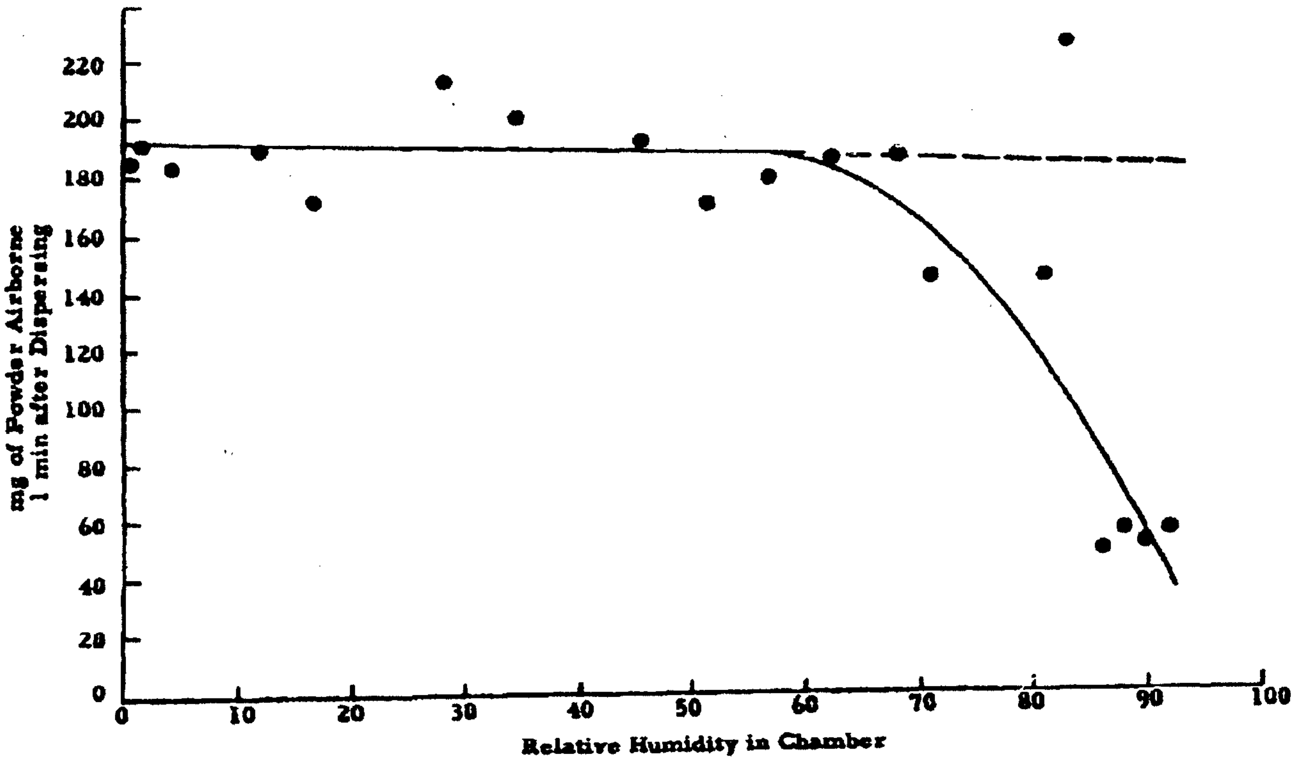

Figure 4. 7. Calculated Mass of Powder Airborne in Initial Aerosol vs. Chamber Humidity

5. DISSEMINATION AND DEAGGLOMERATION STUDIES OF STORED SM

During the fourteenth quarter, tests were completed to determine the effects of storage on the viability and deagglomeration of compacted Sm. Samples of the material were stored at temperatures of -2 and -23C for periods up to six months. The data are being analyzed on a statistical basis at the present time and, therefore, only preliminary results will be presented in this report.

In general, wind-tunnel tests have shown that stored samples can be deagglomerated as efficiently as those that are not stored in the compacted state. Microscopic analyses of filter samples at the six-month period showed that approximately 1.8 percent of all particles observed were agglomerates greater than 4 microns. The aerosols had particle-size distributions characterized by a 0.8 micron MMD and a 3.2 GSD. Approximately 8 percent of all particles observed were greater than 4 microns. From these data it can be concluded that about 20 percent of all particles greater than 4 microns consisted of agglomerates, a value which is in agreement with previous data obtained during this program, and is considered to be small.[15]

Viability assays of the stored materials indicate that the decay rate over the six-month period for each of the treatments is quite similar to the natural decay rate for uncompacted Sm stored at -23C. It appears that the decay rate is higher during the first 15 days of storage than during the following 168 days. Results from the statistical analyses will be presented in the next report.

6. USE OF DRY LUBRICANT TO REDUCE SIDE WALL FRICTION

In the Twelfth and Thirteenth Quarterly Progress Reports, work is reported on the use of dry lubricants to reduce powder-to-metal friction for plugs of compacted powder sliding inside a tube. Most of the experiments were conducted with Mistron Vapor talc packed into 6-inch diameter aluminum tubes. Results with very smooth surfaces indicated that there were no significant differences between the lubricated and unlubricated surfaces. A reduction in frictional force, however, was observed if graphite was applied to the tube wall when various surface roughness conditions existed. A possible explanation is that graphite tends to fill up small scratches and to smooth the surface, thus allowing the plug of compacted talc to slide over the surface with little or no shearing of powder at the interface.

In an effort to learn more about the sliding phenomenon, an experiment was conducted in which the talc-aluminum interface was eliminated by lining the tube with polyethylene film plastic before packing it with talc. Dry graphite was used between the metal and the plastic film to provide lubrication at this point. When the plug of powder was pushed out of the tube it was observed that the plastic liner slid over the graphite-lubricated surface and there was no sliding of powder relative to the plastic.

The length of the plug of talc was 13.5 inches giving a length-to-diameter ratio of 2.25. A force of 150 lb (3.53 psi) was used to compact the talc. The force required to push the plug of powder out of the tube was only 18 lb (0.64 psi). In prior tests, where a graphite-lubricated tube <u>without</u> the plastic liner was filled with talc and compacted at 150 lb (3.53 psi), the ejection force for a length-to-diameter ratio of 2.25 was 150 lb--equal to the compaction force. If it is assumed that the side wall unit pressure is the same in both instances (with and without plastic liner), then it appears that the presence of the plastic film allows the graphite to act as a lubricant, whereas the absence of the plastic film allows the powder particles to somehow seriously degrade the ability of graphite to act as a lubricant.

[redacted]

The surprisingly low side wall friction obtained with the graphite-lubricated film plastic liner demonstrates that, by preventing intimate contact of powder particles with surfaces where relative sliding must take place, it is possible to obtain significant reductions in the side wall frictional resistance. The polyethylene film plastic with graphite lubrication has been employed in a technique for manual loading of the E-41 spray tank with good success (Section 7.2).

It is conceivable that an interface other than plastic film can be developed to be fully effective in lowering side wall friction. Such treatment would be desirable for systems where a continuous plastic film is objectionable, and this matter will be given consideration in planning our future work.

[redacted]

7. PREPARATIONS FOR FLIGHT TESTS OF THE E-41 SPRAY TANK ON THE MOHAWK AIRPLANE

Progress during the reporting period in the planning and preparation for the low-speed flight trials of the E-41 spray tank is summarized below.

7.1. Shipment of E-41 to Grumman Aircraft Engineering Corporation

Late in November the Grumman Airplane Engineering Corporation received authorization to proceed with modifications of a Mohawk OV-1C airplane to permit flying two E-41 spray tanks on this airplane. The pertinent engineering data for the E-41 were sent from General Mills, Inc. to Grumman for use in making the modification. One E-41 spray tank, with associated equipment for ground checkout and operation of the unit, was shipped to Grumman at Bethpage, Long Island, New York, early in December. This unit was filled with approximately 300 lb of Mistron Vapor talc which is to be disseminated during ground checkout at Grumman and during the flight trials at the Naval Air Test Center, Patuxent River, Maryland.

7.2. Manual Technique for Field Loading E-41 Spray Tank with Bg

In connection with the flight trials of the E-41 spray tank on the Mohawk airplane, there was a period when it appeared that only one of the E-41 units would be available for these trials. The other unit had been sent to Eglin Air Force Base and the time for completion of the Eglin trials was indefinite until late in November. With only one unit available for the Mohawk trials it would have been necessary to reload the unit in the field. A partial charge of 80 lb of Bg would constitute the load. The exposure of Bg during loading would have to be minimized to prevent absorption of moisture and to prevent contaminating the area with Bg.

The experiments with a graphite-lubricated polyethylene liner in a 6-inch cylinder with compacted talc (Section 6) demonstrated that it should be possible to develop a packaging arrangement whereby a relatively small force would suffice to push the compacted charge out of the tube that had been used to confine it during compaction. A suitable manual system was developed and demonstrated in the laboratory before it became known that scheduling would permit using both E-41 spray tanks and that Bg loading in the field would not be required.

The arrangement which was developed for loading compacted Bg is sketched in Figure 7-1. The sketch shows the cartridge of powder inside the disseminator prior to removal of the polyethylene liner and the aluminum sleeve. The sleeve is approximately 16.25 inches in diameter so that it slides freely into the disseminator. The central tube is used to provide a hole for the disseminator drive screw and to guide the screw through the polyethylene sleeve in the center.

The polyethylene liner is placed in the aluminum sleeve prior to filling with powder. The film plastic tube in the center is doubled back on itself so that the free end is adjacent to the central tube at the bottom. After the powder is compacted in place, the polyethylene is gathered to the center and tied around the central tube using a special slip-knot. By pulling on this line the knot can be released to free the polyethylene. The polyethylene liner is extra long so that it can be draped back over the tie cord and the outside of the aluminum sleeve. The bottom discs are needed to push the cartridge into the disseminator and to hold the powder in position as the aluminum sleeve and the polyethylene liner are withdrawn.

For the loading operation the disseminator is supported on a rack with the open end tilted about 30 degrees below horizontal. The powder cartridge is inserted and held in place while the release line on the knot is pulled to release the polyethylene. The polyethylene is pulled away from the face of the powder by tugging at the skirt of material extending below the bottom disc. Next, the outer bottom disc is removed so that the aluminum sleeve can be withdrawn while holding the powder in place with the inner bottom disc.

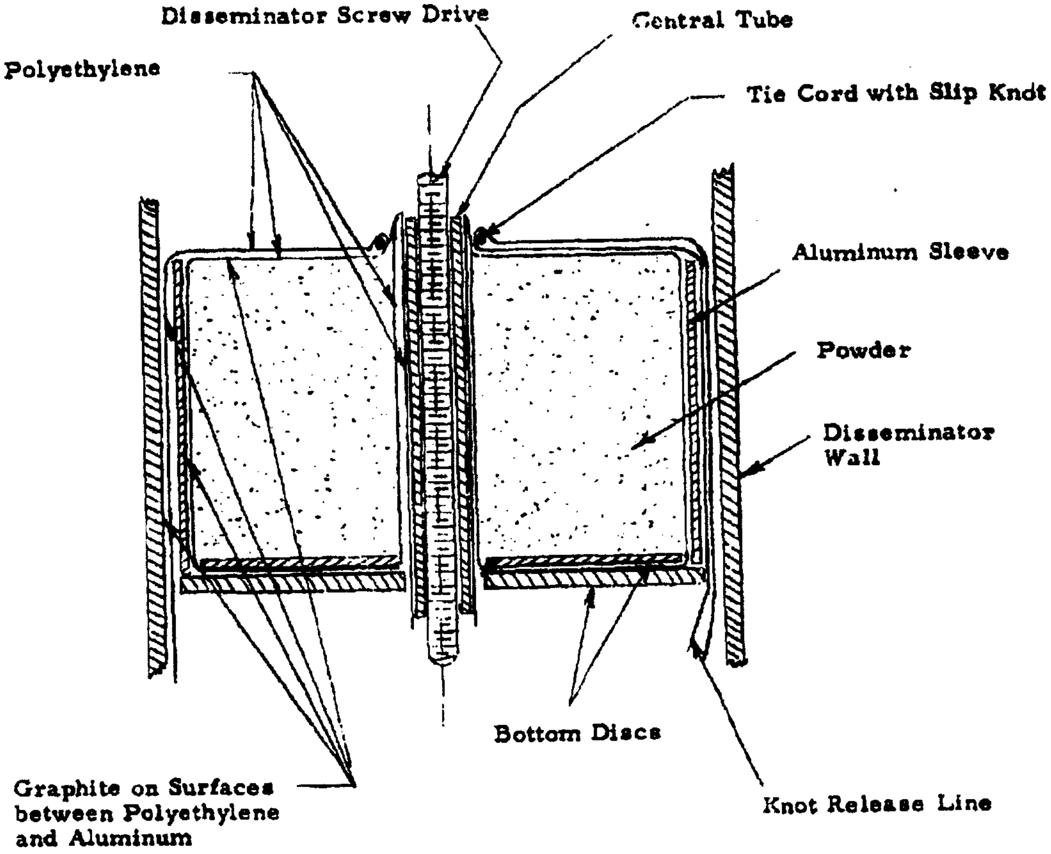

Figure 7-1. Packaging Arrangement for Hand Loading Partial Charge for E-41 Spray Tank

Before removing the inner bottom disc the disseminator is tilted to bring the loading end approximately 30 degrees above horizontal. This maneuver causes the powder to stay in place while the bottom disc is replaced with the disseminator piston and hub assembly.

The technique described above has been found to be entirely satisfactory for loading partial charges where the weight of the cartridge does not exceed that which can be conveniently handled by one man; and when the powder is limited to nonpathogenic simulants. The procedure is easy and no special loading equipment other than the compaction press is required. The polyethylene minimizes the exposure of the powder during the loading operation. The loading cartridge is inexpensive so that it could be destroyed after loading to simplify the decontamination operation when *Bg* is used. The loading cartridge can also serve as a shipping container if packed in a sturdy wooden crate.

8. SUMMARY

The work completed during the fourteenth quarter is summarized in the following paragraphs.

During the course of this project we have been studying the bulk powder properties such as energy of compaction, shear strength, and tensile strength which are manifestations of interparticle contact energies. In addition, we have studied powder particle characteristics such as size and shape that affect the number and nature of these interparticle contacts. Current theoretical investigations relating these interparticle contact energies to mechanical properties of compacted powders are described (Section 2). A theoretical model composed of spherical particles of diameter d_p with an average energy ϵ per contact is employed to determine the energy required to produce a given change in average powder density. Although an idealized system was used, the trends predicted are in accord with experimental data (Section 2).

Bg (lot SCH-63-109) to be used in forthcoming flight tests was found to be more difficult to compact than Bg (lot 17) used previously. A new approach to obtain the energy of compaction from Instron data is presented (Section 2).

Agent LX like other highly elastic materials was found to be difficult to compact, has a comparatively high compaction shear strength, and a tensile strength too low to measure (Section 2).

An evaluation was made of the buoyant force corrections for the BET adsorption method to measure total surface area. Spray-dried saccharin 13C and 13D, agent LX, and egg embryo were found to have total surface areas of 0.78, 1.06, 4.4, and 14.2 with corresponding rugosities of 2.0, 2.2, 6.8, and 26.8. Spray-dried saccharin is composed of smooth spheres, whereas the egg embryo and agent LX is a highly irregularly shaped elastic particle as shown in the micrographs (Section 3). Our methods for preparing shadow-cast samples for the electron microscope are described (Section 3).

A study of the effects of humidity (from 0 to 100 percent R. H.) upon the formation and decay of a ground powdered sugar aerosol is reported in Section 4. The data were thoroughly analyzed, consistent with the test parameters designated in the method of measuring aerosol decay by light-scattering techniques. The results indicate that pronounced changes probably do not occur until the relative humidity is greater than 65 percent.

Viability and deagglomeration studies were conducted on samples of compacted Sm that had been stored in the compacted state for a period of 6 months at temperatures of -2 and -23°C. Wind-tunnel tests showed that these samples were deagglomerated as efficiently as compacted Sm that had not been stored. Viability assays have not been completely analyzed but indications are that decay rates for six months of storage are similar for compacted and uncompacted Sm (Section 5).

An experiment was conducted using Mistron Vapor talc compacted in a 6-inch diameter tube wiped with graphite and lined with polyethylene film plastic. The force required to push the plug of talc out of the tube was appreciably less than has been observed for similar plugs without the polyethylene, indicating that side-wall friction can be materially reduced if suitable methods can be found for preventing intimate contact of the powder particles with the wall surface (Section 6).

In preparation for the low-speed flight trials of the E-41 spray tank on the Mohawk OV-1C airplane, an E-41 was filled with compacted talc and shipped to Grumman Aircraft Engineering Corporation, Bethpage, Long Island, New York. A manual loading technique using partial charges was developed in anticipation of having to load the E-41 with Bg in the field during the flight trials (Section 7).

9. REFERENCES

1. Jenkin, C. F. Proc. Roy. Soc. (London). A 131: 53-89 (1931).

2. Zenz, F. A. and D. F. Othmer. Fluidization and fluid particle systems. N. Y., Reinhold, 1960.

3. Deriagin, B. V. and I. I. Abrikosova. Soviet Phys. JETP 3:819 (1956).

4. U. S. Army Chemical Corps. Biological Warfare Laboratories. Technical Memo. 9-22. Mathematical model for energy of compaction of a bed of powder, by J. S. Derr (November 1960).

5. Lindsay, R. B. Concepts and methods of theoretical physics. Princeton, New Jersey, Van Nostrand, 1951.

6. General Mills, Inc. Electronics Division. Report no. 2344. Dissemination of solid and liquid BW Agents (U), by G. R. Whitnah. Contract DA-18-064-CML-2745. Ninth Quarterly Progress Report (October 19, 1962. Confidential.

7. ---- Report no. 2411 ... Twelfth Quarterly Progress Report (July 10, 1963). Confidential.

8. ---- Report no. 2451 ... Thirteenth Quarterly Progress Report (October 17, 1963). Confidential.

9. ---- Report no. 2395 ... Eleventh Quarterly Progress Report (May 4, 1963). Confidential.

10. Hall, C. E. Introduction to electron microscopy. N. Y., McGraw-Hill, 1953. p. 329.

11. Fischer, R. B. Applied electron microscopy. Bloomington, Indiana University Press, 1954. p. 109.

12. White, L. J. and G. J. Duffy. Vapor-phase production of colloidal silica. Ind. Eng. Chem. 51: 232-38 (1959).

13. General Mills, Inc. Electronics Division. Report no. 2322. Dissemination of solid and liquid BW Agents (U), by G. R. Whitnah. Contract DA-18-064-CML-2745. Eighth Quarterly Progress Report (August 22, 1962). Confidential.

14. ---- Report no. 2373 ... Tenth Quarterly Progress Report (February 4, 1963). Confidential.

15. ---- Report no. 2264 ... Sixth Quarterly Progress Report (February 23, 1962). Confidential.

DEPARTMENT OF DEFENSE
WASHINGTON HEADQUARTERS SERVICES
1155 DEFENSE PENTAGON
WASHINGTON, DC 20301-1155

MEMORANDUM FOR DEFENSE TECHNICAL INFORMATION CENTER
(ATTN: WILLIAM B. BUSH)
8725 JOHN J. KINGMAN ROAD, STE 0944
FT. BELVIOR, VA 22060-6218

AUG 1 2013

SUBJECT: OSD MDR Cases 12-M-3144 through 12-M-3156

At the request of [redacted], we have conducted a Mandatory Declassification Review of the documents in the above referenced cases on the attached Compact Disc (CD) under the provisions of Executive Order 13526, section 3.5, for public release. We have declassified the documents in full. We have attached a copy of our response to the requester. If you have any questions, please contact Ms. Luz Ortiz by phone at 571-372-0478 or by e-mail at luz.ortiz@whs.mil, luz.ortiz@osd.smil.mil, or luz.ortiz@osdj.ic.gov.

Robert Storer

Robert Storer
Chief, Records and Declassification Division

Attachments:
1. MDR request w/ document list
2. OSD response letter
3. CD (U)

April 26, 2012

[redacted]

Department of Defense
Directorate for Freedom of Information and Security Review
Room 2C757
1155 Defense Pentagon
Washington, D.C. 20301-1155

Sir:

I am requesting under the Mandatory Declassification Review provisions of Executive Order 13291, copies of the following documents. I have tried several times to acquire them through DTIC, but the sites stated they are not available.

I am conducting research into the previous methods used to disseminate biological agents. Many source I use to have access to have been deleted from the internet. On numerous occasions I have been informed that formerly classified information that was declassified, have now become classified again (since 911). My attempts to locate such Executive Orders, regulations, laws, or other changes to this question have not successful nor revealed a specific source. As such I would appreciate any information you can shed on this question.

Documents requested.

AD 348405, Dissemination of Solid and Liquid BW (Biological Warfare)Agents Quarterly 12-M-3144
Progress Report Number 14, 4 Sept - 4 Dec 1963, G. R. Whitnah, February 1964, General Mills Report number 2512, General Mills, Inc., Minneapolis, MN, Contract number DA 18064 CML 2745,102pages. Prepared for U.S. Army Biological Laboratories, Fort Detrick, Maryland. Approved by S.P. Jones, Director of Aerospace Research at General Mills. Project No. 82408. General Mills Aerospace Research Division, 2295 Walnut Street, St. Paul 13,Minnesota.
AD 346751, Dissemination of Solid and Liquid BW (Biological Warfare) Agents, Quarterly 12-M-3145
Progress Report Number 12, March 4 - June 4, 1963, G. R. Whitnah, July 1963, General Mills Report number 2411, General Mills, Inc., Minneapolis, MN, Contract number DA 18064 CML 2745. 184 pages. Approved by S.P. Jones, Director of Aerospace Research at General Mills. Project No. 82408. General Mills Aerospace Research Division, 2295 Walnut Street, St. Paul 13, Minnesota.
AD 346750, Dissemination of Solid and Liquid BW (Biological Warfare) Agents, Quarterly 12-M-3146
Progress Report Number 13, 4 June - 4 Sept 1962, G.R. Whitnah, October 1963, General Mills

12-M-3144

Report number 2451, General Mills, Inc., Minneapolis, MN, Contract Number DA 18064 CML 2745. 19 pages (?)

12-M-3147 AD 332404, Dissemination of Solid and Liquid BW (Biological Warfare) Agents, Quarterly Progress Report Number 7, Dec. 4, 1961 - March 4, 1962, by G.R.Whitnah, February 1963, General Mills Report Number 2373, General Mills, Inc., Minneapolis, MN, Contract Number DA 18064 CML 2745. 123 pages.

12-M-3148 AD 333298, Dissemination of Solid and Liquid BW (Biological Warfare)Agents, Quarterly Progress Report Number 9, June 4, 1962 - Sept. 4, 1962. by G.R. Whitnah, October 1962, General Mills Report Number 2344, General Mills, Inc., Minneapolis, MN, Contract Number DA 18064 CML 2745. 130 (or 150) pages.

12-M-3149 AD 332405, Dissemination of Solid and Liquid BW (Biological Warfare) Agents, Quarterly Progress Report Number 8, Period March 4, 1962 - June 4, 1962. G.R. Whitnah, August 1962, General Mills Report Number 2322, General Mills, Inc., Minneapolis, MN, Contract Number DA 18064 CML 2745. 198 pages.

12-M-3150 AD 329067, Dissemination of Solid and Liquid BW (Biological Warfare) Agents, Quarterly Progress Report Number Six, G.R. Whitnah, February 1962, General Mills Report Number 2264, General Mills, Inc., Minneapolis, MN, Contract Number DA 18064 CML 2745. 103 pages. Approved by S.P. Jones, Manager, Materials and Mechanics Research, General Mills Research and Development Office, 2003 East Hennepin Avenue, Minneapolis 13, Minnesota.

12-M-3151 AD 327072, Dissemination of Solid and Liquid BW (Biological Warfare) Agents, Quarterly Progress Report Number Five, 4 June - 4 Sept 1961. by G.R.Whitnah, November 1961, General Mills Report Number 2249, General Mills, Inc., Minneapolis, MN, Contract Number DA 18064 CML 2745.

12-M-3152 AD 325247, Dissemination of Solid and Liquid BW (Biological Warfare) Agents, Quarterly Progress Report Number 4, 4 March - 4 June 1961, by J.E. Upton for G.R. Whitnah, Project Manager. February 1963, General Mills Report Number 2216, General Mills, Inc., Minneapolis, MN, Contract Number DA 18064 CML 2745. General Mills Electronics Group, Research Dept., 2003 East Hennepin Avenue, Minneapolis 13, Minnesota. 225 pages.

12-M-3153 AD 324746, Dissemination of Solid and Liquid BW (Biological Warfare) Agents, Progress Report 3 Juen - 3 Sept. 1960. by G.R. Whitnah, October 1960, General Mills Report Number 2125, General Mills, Inc., Minneapolis, MN, Contract Number DA 18064 CML 2745. 78 pages

12-M-3154 AD 323599, Dissemination of Solid and Liquid BW (Biological Warfare) Agents, Quarterly Progress Report Number 2, for period 4 Sept - 4 Dec 1960, by G.R. Whitnah, February 1961, General Mills Report Number 2161, General Mills, Inc., Minneapolis, MN, Contract Number DA 18064 CML 2745. 90 pages? Mechanical Division of General Mills, Inc., Research Department, 2003 East Hennepin Avenue, Minneapolis 13, Minnesota.

AD 323598, Dissemination of Solid and Liquid BW (Biological Warfare) Agents, Quarterly Progress Report, for period 4 Dec. 1960 - 4 March 1961, by G.R. Whitnah, May 1961, General Mills Report Number 2200, General Mills, Inc., Minneapolis, MN, Contract Number DA 18064 CML 2745. 95 pages. 12-M-3155

AD 337635, Dissemination of Solid and Liquid BW (Biological Warfare) Agents, Quarterly Progress Report No. 10, period Sept. 4, 1962 - Dec. 4, 1962. G.R. Whitnah, Project Manager, Approved by S.P. Jones, Aerospace Research, February 1963. 247 pages. 12-M-3156

Sincerely

[redacted]